[redacted]

HUGHES

HUGHES AIRCRAFT COMPANY

FQ7-41107

REF. NO.: 2242/3667
23 April 1964

SURVEYOR THRUST PHASE FLIGHT CONTROL SYSTEM

by

G. E. O'Connor
H. D. Marbach

H. D. Marbach

G. E. O'Connor

APPROVED:
O. N. Hermann

This work was performed for the Jet Propulsion Laboratory, California Institute of Technology, sponsored by the National Aeronautics and Space Administration under Contract NAS7-100.

1. CONTENT AND ORGANIZATION

1.1 Description of the Surveyor Mission

1.1.1 Purpose of the Mission: The purpose of the Surveyor mission is to soft land a package of scientific instruments on the surface of the moon, and to carry out a series of experiments with these instruments. The landing site is preselected, and is to be hit with a 3σ landing dispersion of less than 67 km.

1.1.2 Sequence of Events: The mission is carried out as follows:

1. The spacecraft is boosted into an earth-moon trajectory by an Atlas-Centaur combination.

2. The spacecraft is separated from the booster.

3. The spacecraft attitude rates imparted by the separation operation are nulled out by cold gas jet control torques commanded by suitably processed signals from three body-fixed rate integrating gyros.

4. Spacecraft attitude is locked up on the Sun and Canopus. This is achieved and verified by a series of programmed maneuvers commanded from Earth. Attitude reference is provided by optical Sun and Canopus sensors, and the integrating gyros. Control torques are provided by the cold gas jets.

5. The spacecraft continues along its trajectory in this mode until the mid-course correction takes place. During this period the JPL Space Flight Operations Facility (SFOF) determines the actual spacecraft trajectory and computes the velocity increment needed to correct the actual trajectory to the desired trajectory.

6. The spacecraft roll axis is then pointed in the direction of the desired velocity increment. This is accomplished by programmed commands from Earth to the cold gas jet control system.

7. The three vernier rocket engines are ignited and thrust at a precisely controlled period of time. The thrust level (more precisely the thrust-to-mass ratio) is controlled by throttling the vernier engines with the error between a precise command voltage and an accelerometer. The time period is controlled by a digital clock which is preset and verified from Earth in accordance with the velocity increment computation. Pitch/yaw attitude is controlled by differential throttling of the three vernier engines with suitably processed signals from the pitch and yaw

7. (continued)

gyros. Roll control is achieved by gimballing one of three vernier engines in accordance with a suitably processed signal from the roll gyro

8. At the end of the programmed thrusting period, the digital clock shuts down the three vernier engines. Spacecraft attitude is once more locked up on the Sun and Canopus by the cold gas jet system.

9. The spacecraft continues along its trajectory in this mode until the main retrorocket phase. During this period SFOF again determines the actual spacecraft trajectory.

10. The spacecraft roll axis is then pointed close to the direction of the spacecraft velocity vector. This is accomplished, as was Step 6, on command from Earth.

11. The altitude marker radar AMR) generates a signal when the slant range from the spacecraft to the lunar surface is approximately 55 miles. This signal starts a digital clock.

12. After an interval of time pre-commanded from Earth, the digital clock ignites the vernier rocket engines.

13. One second after the vernier engine ignition signal, the digital clock ignites the main retrorocket.

14. The spacecraft continues along its trajectory with the main retrorocket thrusting until main retrorocket burnout. During this period attitude is controlled as in Step 7

15. Main retrorocket burnout is sensed by a g-switch which closes when spacecraft acceleration falls below 3.5 (lunar) g's.

16. The g-switch signal starts a digital clock and commands near-maximum vernier engine thrust.

17. After a fixed time delay the digital clock fires the explosive bolts which fasten the main retrorocket case to the spaceframe.

18. After another fixed time delay, the digital clock enables the vernier phase control system.

19. When the radars generate signals indicating that they are operating properly, the vernier phase control system is turned on. In this control mode the radars generate signals which continually maintain alignment between the spacecraft velocity vector and the spacecraft roll axis, and which control thrust to maintain a preprogrammed slant range vs. velocity trajectory.

20. When slant range has decreased to 1000 feet, the radar altimeter generates a digital signal marking that range, and changes its analog output voltage scale factor to provide better resolution at low altitudes. The flight control system utilizes the 1000 foot mark to trigger a change in gain in the Doppler attitude channels and a change in the descent command profile.

21. When the Z-axis velocity has decreased to 10 ft/sec, a trigger in the flight control electronics reacts to the Doppler Velocity Sensor Z-axis analog output to produce a digital signal. This digital signal removes the Doppler attitude signals and commands a constant Z-axis velocity of 5 ft/sec.

22. The spacecraft descends at a constant velocity of 5 ft/sec. During this period attitude is held fixed.

23. When slant range has decreased to 13 feet the radar generates a digital signal marking that range. This signal is utilized by the flight control electronics to shut down the three vernier rocket engines.

24. The spacecraft free falls to touchdown.

1.2 Description of Flight Control System: The Surveyor flight control system consists of sensors, electronic amplifiers and switches, and actuators. The flight control electronics selects and processes signals from the sensors suitable to the several phases of the mission. The processed signals are used to command control forces from the appropriate actuators. Table 1.2.1 lists the sensors and actuators used in the several phases of the mission. The phases of the flight are identified by the numbers assigned to them in section 1.1.2. This report is intended to be a detailed account of the design of the flight control systems used during phases 7, and 12 through 23. The control systems used in the other phases are described in detail in Reference 1.

1.3 Organization of Report: The remainder of this report will follow the following pattern:

1. A detailed sequence of events;
2. A detailed description of thrust phase control system configurations;
3. A description of the considerations which lead to the current system design.

Table 1.2.1

Phase	Sensors	Actuators
3, 6, 10	Pitch, yaw and roll gyros	Cold gas jets
4, 5, 8, 9	Sun and Canopus sensors; pitch, yaw, and roll gyros	Cold gas jets
7	Pitch, yaw and roll gyros; accelerometer	Vernier rocket engines, roll actuator
11	Pitch, yaw and roll gyros; altitude marking radar	Cold gas jets
12	Pitch, yaw and roll gyros	Vernier rocket engines, roll actuator
13, 14, 15, 16, 17	Pitch, yaw and roll gyros; g-switch	Vernier rocket engines, roll actuator, main retrorocket engine
18, 19, 20, 21, 22, 23	Pitch, yaw and roll gyros; accelerometer; radar altimeter and Doppler velocity sensor	Vernier rocket engines, roll actuator

2.0 SEQUENCE OF EVENTS

2.1 Midcourse Correction: The midcourse velocity correction (phases 6, 7 and 8 of Section 1.1.2) is carried out as follows:

1. The spacecraft is maneuvered to the desired attitude.
2. The digital clock is set by radio command from Earth.
3. The vernier rocket engines are lighted and the digital clock is started.
4. The vernier rocket engines thrust at a precisely controlled thrust-to-mass ratio.
5. The digital clock shuts down the vernier rocket engines at the end of the preset thrusting period.
6. Spacecraft attitude is maneuvered back to lock-up on the Sun and Canopus.

2.2 Main Retrorocket Phase: The main retrorocket phase (phases 10 through 18 of Section 1.1.2) is carried out as follows:

1. Nominal vernier rocket engine thrust level for the main retrorocket phase is radio commanded from Earth.
2. The spacecraft is maneuvered to the desired attitude.
3. The digital clock is set by radio command from Earth.
4. At a slant range from the lunar surface of approximately 55 miles, the altitude marking radar generates a signal which starts the digital clock.
5. At the end of the preset period, the digital clock generates a signal which ignites the vernier rocket engine.
6. One second after the vernier rocket engine ignition signal, the digital clock generates a signal which ignites the main retrorocket engine.
7. The main retrorocket thrusts until it burns out. Burnout is detected by a g-switch. When spacecraft deceleration has decreased to 3.5 g's, the g-switch generates a signal which starts a digital clock.
8. After 8 seconds, the digital clock generates a signal which explodes the bolts which fasten the main retrorocket case to the spaceframe. Simultaneously, near-maximum vernier rocket engine thrust is commanded.

9. Two seconds after the bolts are exploded, the digital clock commands near minimum vernier rocket engine thrust and enables the vernier phase control system.

2.3 Vernier Phase: The vernier phase (phases 18 through 23) is carried out as follows:

1. When both the Reliable Operate-Radar Altimeter (RORA) and the Reliable Operate-Doppler Velocity Sensor (RODVS) signals appear, the vernier phase control system is turned on. A combination of RORA and Conditional Reliable Operate-Doppler Velocity Sensor (CRODVS) signals will also turn on the vernier phase control system. The RORA, RODVS, and CRODVS signals are digital indicators which are generated by the radars. They indicate that the analog radar signals are being generated properly. The CRODVS signal indicates that the Doppler velocity signals are not in specification, but are sufficiently accurate to be used for a preliminary attitude correction.

2. The spacecraft descends along a preprogrammed trajectory to a slant range of 1000 feet. At this point the radar generates a digital signal marking this range. This signal operates switches in the flight control electronics which change several electronic parameters to values suitable for lower altitudes and velocities.

3. The spacecraft descends along the preprogrammed trajectory until its velocity decreases to 10 feet per second. At that point a trigger in the flight control electronics reacts to the Z-axis Doppler Velocity Sensor analog output to produce a digital signal which commands the spacecraft to descent at a constant velocity of 5 fps and at a fixed attitude.

4. When slant range has decreased to 13 feet, the radar altimeter generates a digital signal marking that range. This signal operates switches in the flight control electronics which shut down the vernier rocket engines.

3.0 CONTROL SYSTEM CONFIGURATION

3.1 Spacecraft Coordinate System: The spacecraft X, Y, Z (pitch, yaw and roll respectively) axes are a right-handed rectangular coordinate system defined by tooling fixtures (see Reference 2). Nominally, the origin of this system lies at the spacecraft center of mass, the Z-axis points in the direction of rocket engine exhaust, and the Y-axis passes through leg 1 of the spacecraft. The +Y direction is toward leg 1.

3.2 Vernier Rocket Engine Configuration: Figure 3.2.1 shows the physical arrangement of the three vernier rocket engines relative to the X, Y, Z axes. Note that engine No. 1 is gimballed for roll control.

3.3 Sensor Configuration

3.3.1 Gyro Configuration: Three integrating gyros are body-fixed to produce analog output signals proportional to the integral of body rates about the X, Y, and Z axes.

3.3.2 Accelerometer: The accelerometer is mounted so that it measures the thrust-to-mass ratio in the Z-direction.

3.3.3 Altitude Marking Radar: The AMR is mounted so that it generates a digital signal when the distance from the spacecraft to the lunar surface, as measured along the Z-axis, is approximately 55 miles.

3.3.4 Radar Altimeter and Doppler

3.3.4.1 Velocity Sensor: The Radar Altimeter and Doppler Velocity Sensor (RADVS) produce analog signals proportional to spacecraft velocity components in the X, Y, and Z-directions, and the distance to the lunar surface is measured along the Z-axis (slant range). In addition, the radar altimeter generates digital signals when slant range reaches 1000 feet and 13 feet.

3.4 Thrust Phase Control System Configuration During Midcourse Velocity Correction: Figure 3.4.1 shows the control system hardware configuration during the midcourse thrusting period (phase 7 of Section 1.1.2). This control system operates roughly as follows. The acceleration signal amplifier produces a throttling command which tends to null the difference between the acceleration command voltage and the accelerometer signal. The pitch and yaw shaping amplifiers produce pitch and yaw control moment commands which tend to null the respective gyro analog outputs. The mixing network generates uniform throttling commands to the three engines proportional to the acceleration signal amplifier output and differential throttling commands proportional to the pitch and yaw shaping amplifier outputs. The servo loops thus instrumented are shown in Figures 3.4.2 and 3.4.3 and 3.4.4. The loop shown in Figure 3.4.2 will henceforth be referred to as the roll control loop, that in Figure 3.4.3 as the inner rate loop, and that in Figure 3.4.4 as the acceleration loop. There are actually two identical inner rate loops. One contains the pitch gyro, the pitch shaping amplifier, and the pitch moment of inertia. The other contains the yaw gyro, the yaw shaping amplifier, and the yaw moment of inertia. The four loops described above are very

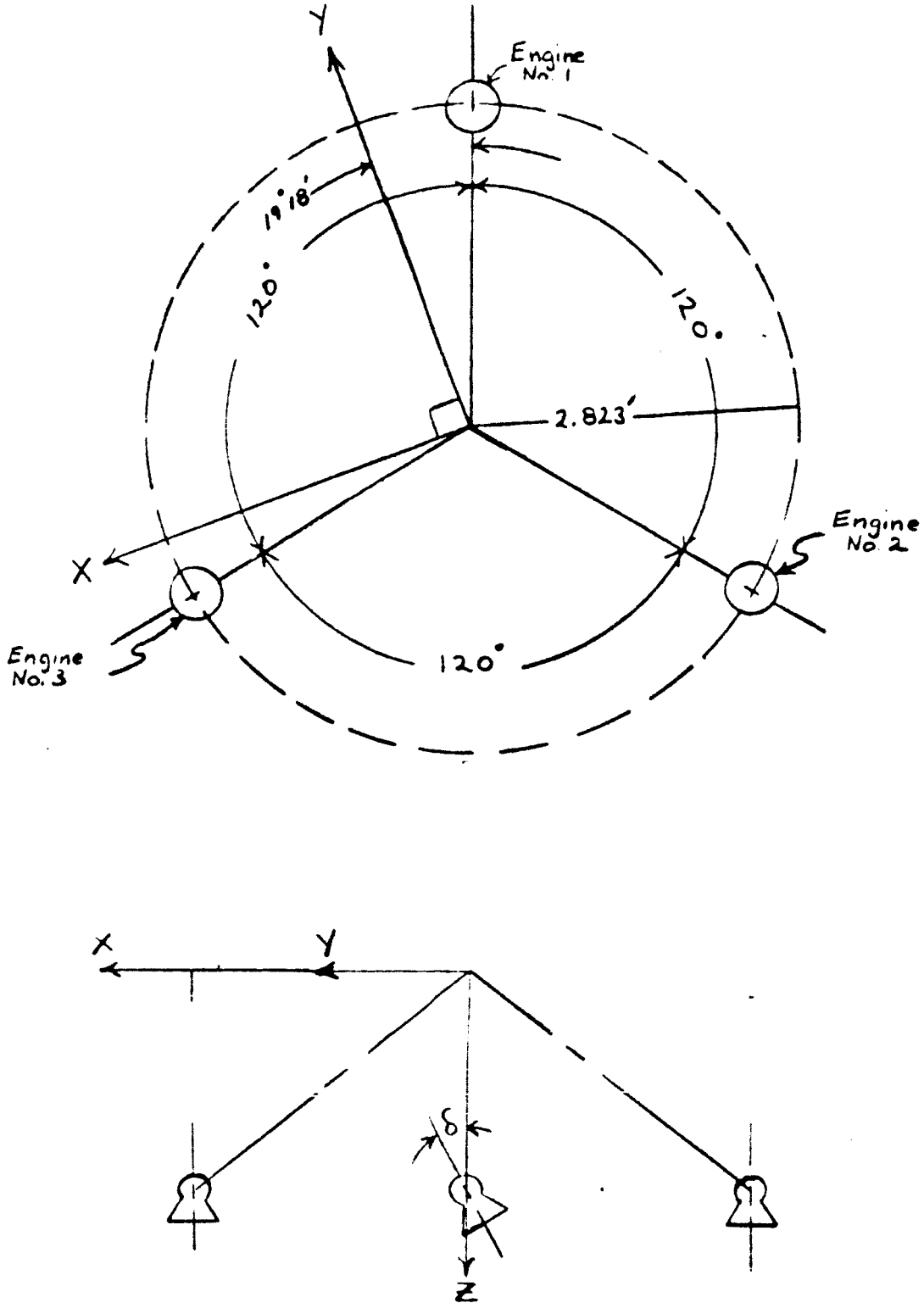

FIGURE 3.2.1 Vernier Engine Configuration

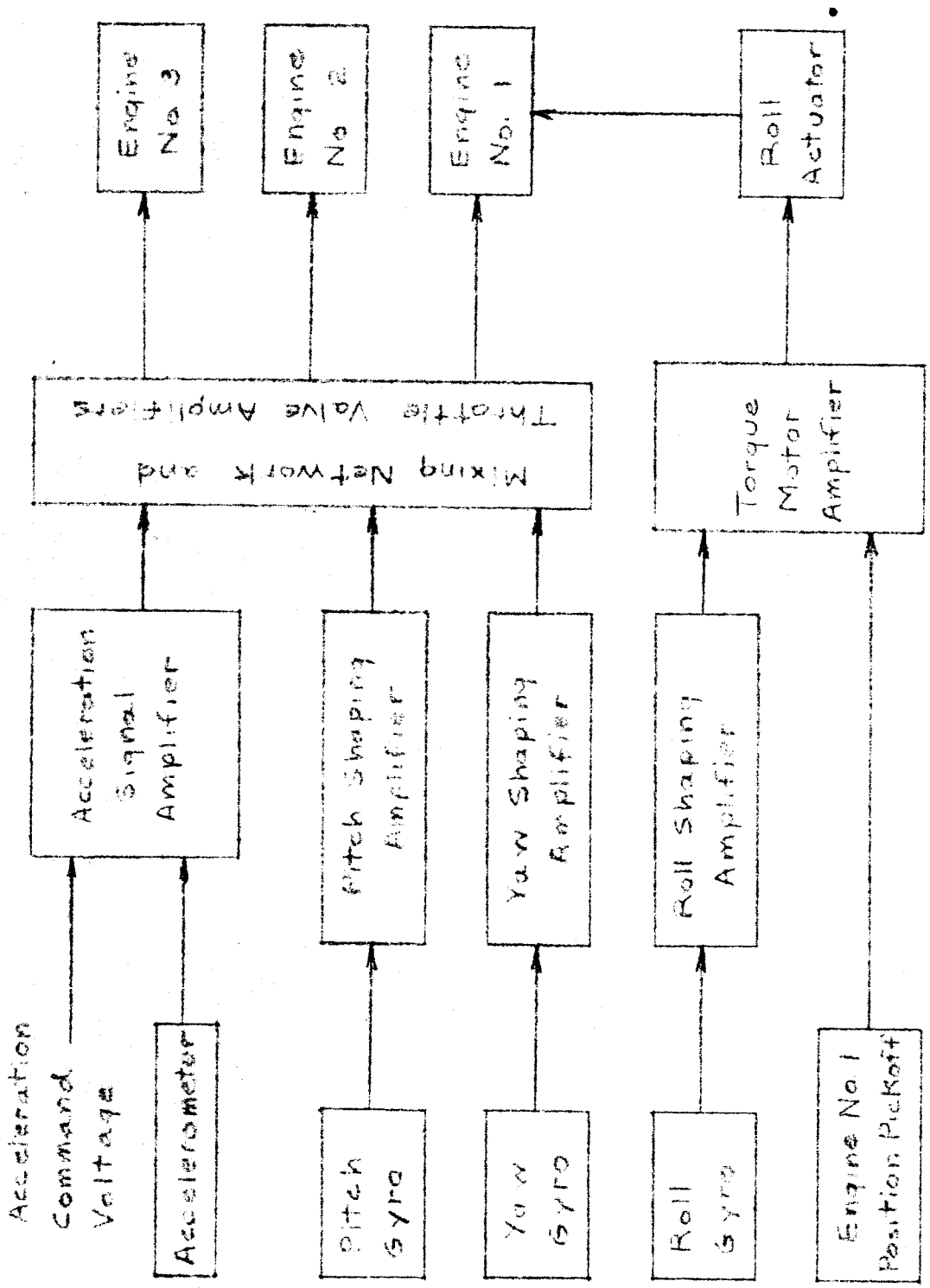

Figure 3.4.1 - Midcourse Thrust Period Configuration

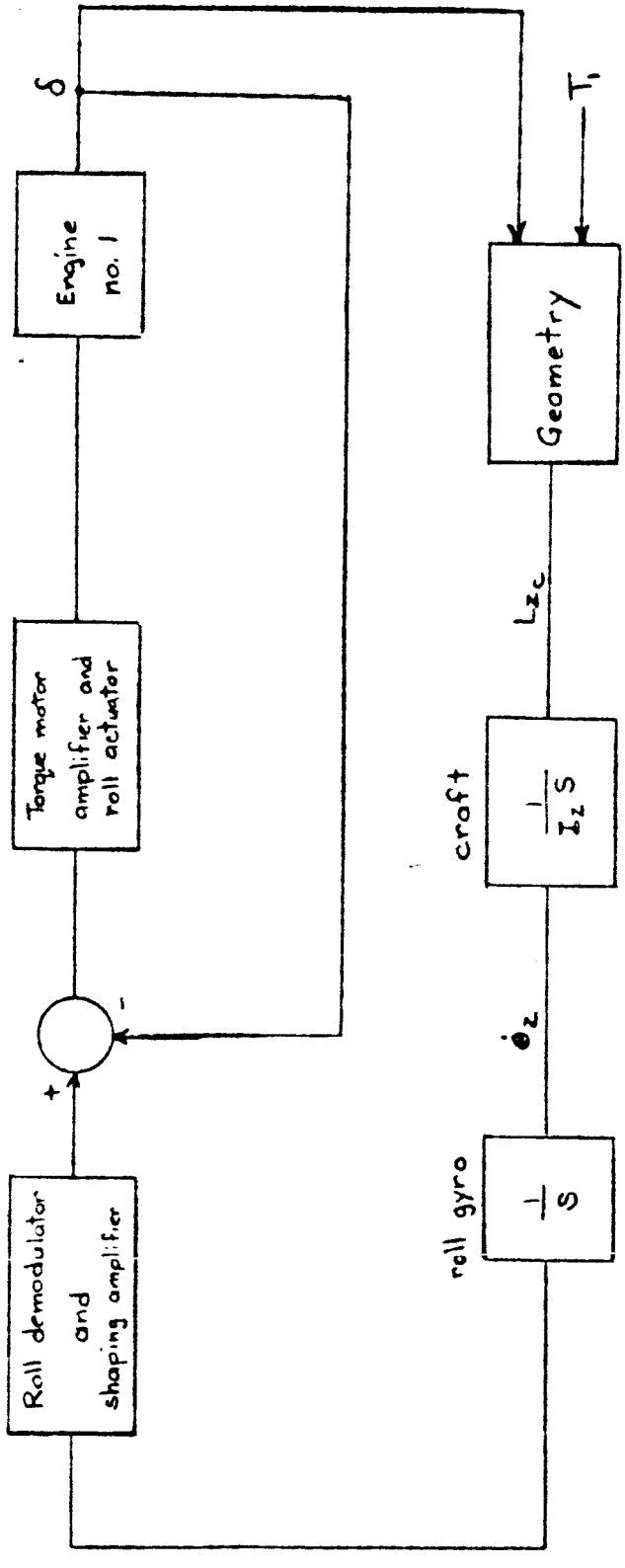

FIGURE 3.4.2 Roll Control Loop

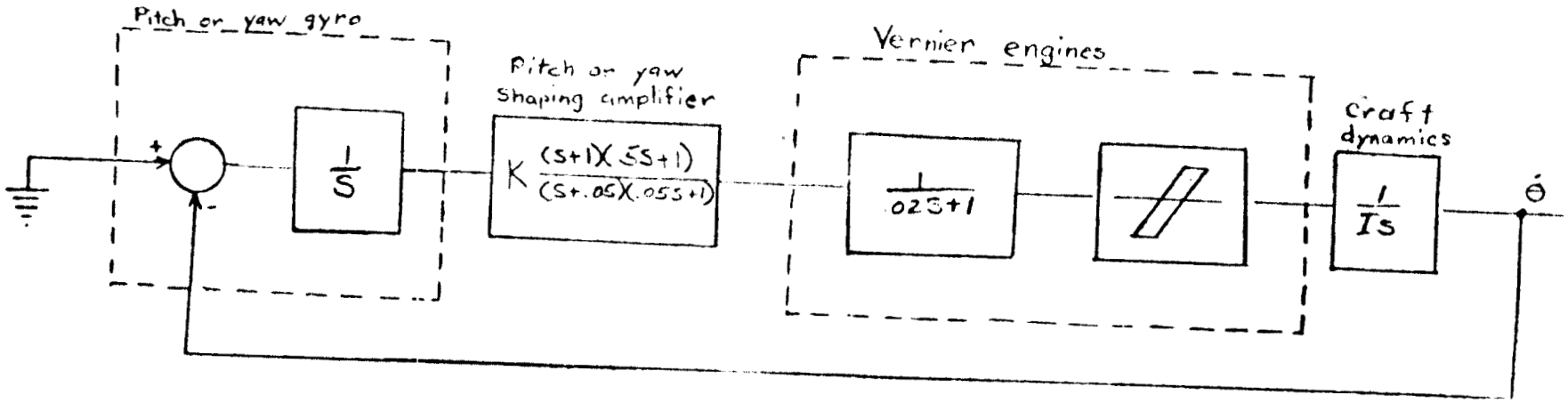

FIGURE 3.4.3 Inner Rate Loop

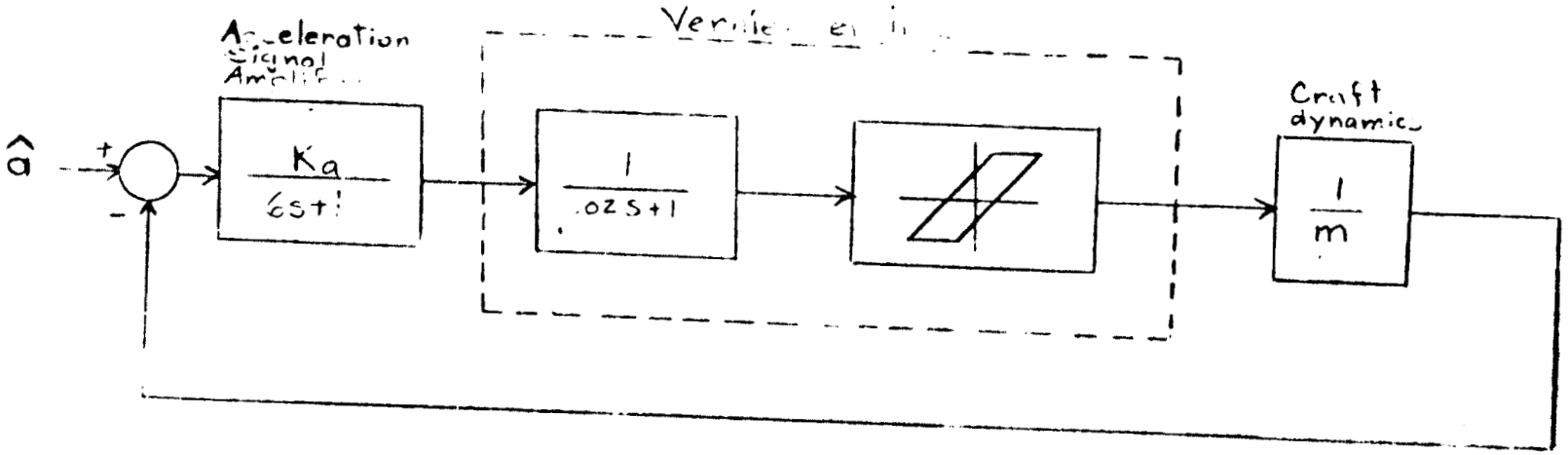

FIGURE 3.4.4 Acceleration Loop

nearly uncoupled because of spacecraft inertial symmetry. The expected cross-coupling between loops has been investigated and found to be negligible.

3.5 Main Retrorocket Phase Control System Configuration: The main retrorocket phase control system configuration is identical to that of the thrust phase midcourse velocity correction control system, except that the accelerometer is not used. Thus, the acceleration loop is open, and vernier engine thrust level is commanded by a fixed voltage into the mixing network. The reason for not using the accelerometer is that it does not have sufficient dynamic range to operate when the main retrorocket is thrusting.

3.6 Vernier Phase Control System Configuration: Figure 3.6.1 shows the control system hardware configuration during the vernier phase (phases 19 through 23 of Section 1.1.2). Also shown is the switching system which sets up the various control modes. The vernier phase control system consists of two separate subsystems, the attitude control system and the trajectory control system. These are described separately in the succeeding sections.

3.6.1 Vernier Phase Attitude Control: The vernier phase attitude control system operates roughly as follows: From the time that the RODVS or CRODVS signal appears until the time that the Z-axis velocity reaches 10 fps, the X and Y velocity signals from the Doppler Velocity Sensor are used to command pitch and yaw body rates which tend to null the X and Y velocity components. This keeps the Z-axis aligned to the velocity vector. When the Z-axis velocity reaches 10 fps, the Doppler steering signals are removed from the gyros, and attitude is held fixed for the remainder of the vernier phase. A servo loop diagram of the pitch channel is shown in Figure 3.6.2. The yaw channel is identical. The roll control system is that described in Section 3.4.

3.6.2 Vernier Phase Trajectory Control: The vernier phase trajectory control system operates roughly as follows: From the time that both RODVS and RORA signals appear until Z-axis velocity is reduced to 10 fps, the spacecraft descent is controlled to follow a preprogrammed slant range vs. Z-axis velocity profile. This is accomplished as follows: The slant range analog signal from the radar altimeter is fed into an analog segmental approximation to the desired descent profile. This analog of the desired descent profile generates a velocity command corresponding to the slant range input. This velocity command is differenced with the Z-axis velocity analog signal from the Doppler velocity sensor. The resulting error signal is used to control spacecraft acceleration, so that the error signal is nulled. When Z-axis velocity has been reduced to 10 fps, a constant velocity command of 5 fps is substituted for that from the descent trajectory analog. Figure 3.6.3 shows a servo loop diagram of the vernier phase trajectory control system.

3.7 Switching System: The switching system operates as follows (switch numbers refer to Figure 3.6.1): Switches 2p and 2y turn on the Doppler attitude system. They are closed by an "and" gate whose inputs are the delayed delayed burnout signal, the Doppler reliable signal, the thrust phase power ON signal, and the absence of the 10 fps detector signal. Switches 7p and 7y serve to set zero initial conditions on analog integrators

in the pitch and yaw shaping amplifiers. They are closed when thrust phase power is turned on, but opened when the vernier engine ignition signal appears.

Switch 11 turns on the trajectory control system described in Section 3.6.2. It is closed by an "and" gate whose inputs are the thrust phase power ON signal, the RODVS signal, and the RORA signal. Switches 13, 14, and 15 are used to select the proper velocity command. Switch 13 is closed for slant range above 1000 feet. Switch 14 closed for slant range below 1000 feet, and Z-axis velocity above 10 fps. Switch 15 is closed for Z-axis velocity below 10 fps.

Switch 9 supplies the midcourse acceleration command. It is closed only during the midcourse velocity correction phase. Switch 12 supplies a minimum acceleration command to the acceleration loop during the vernier phase. It is closed by the delayed delayed burnout signal. Switch 10 sets an initial voltage of zero on a capacitor in the acceleration signal amplifier. It is closed when thrust phase power is turned on, but opened when the midcourse ignition signal or the delayed delayed burnout signal appears.

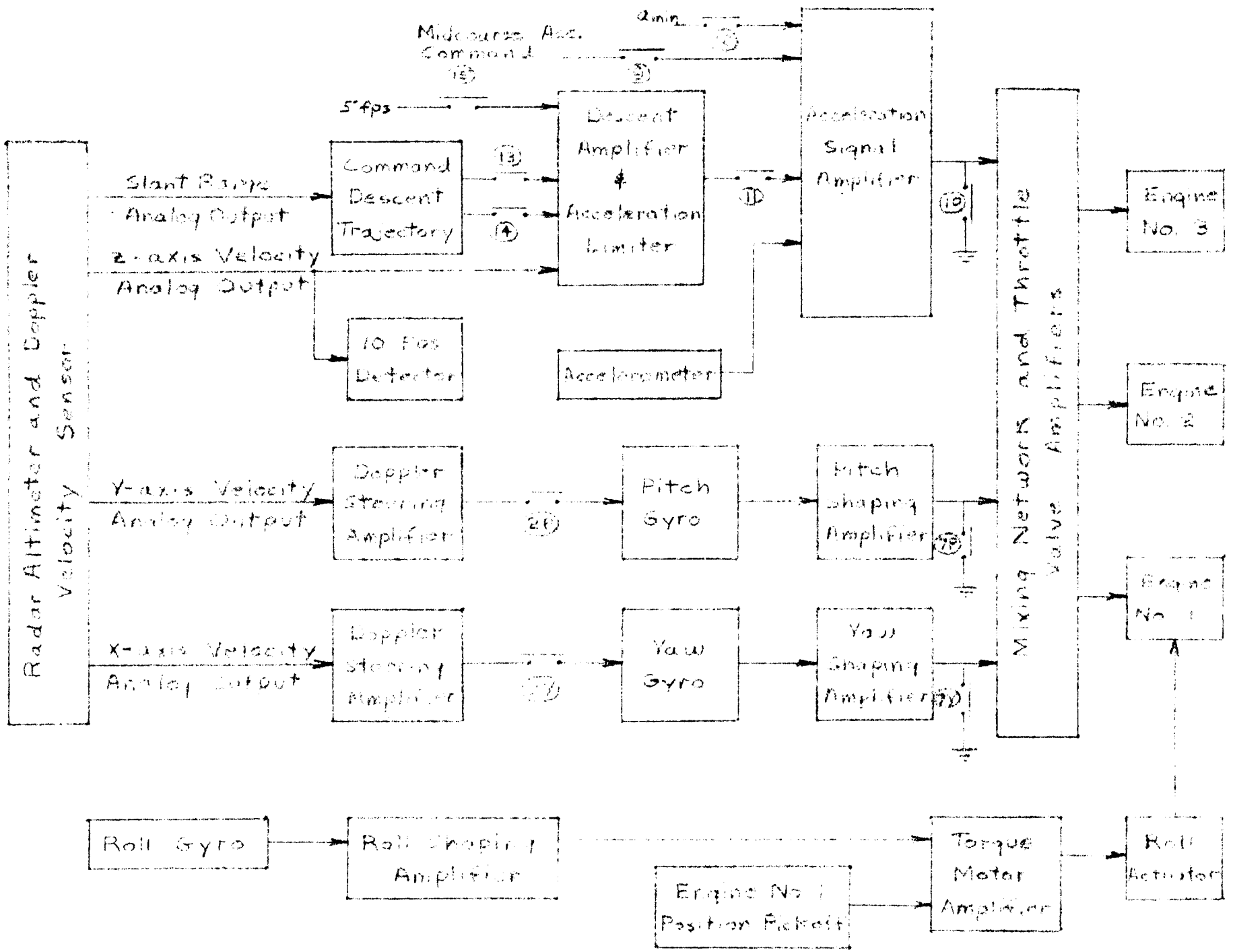

Figure 3.6.1 - Vernier Phase Control System Configuration

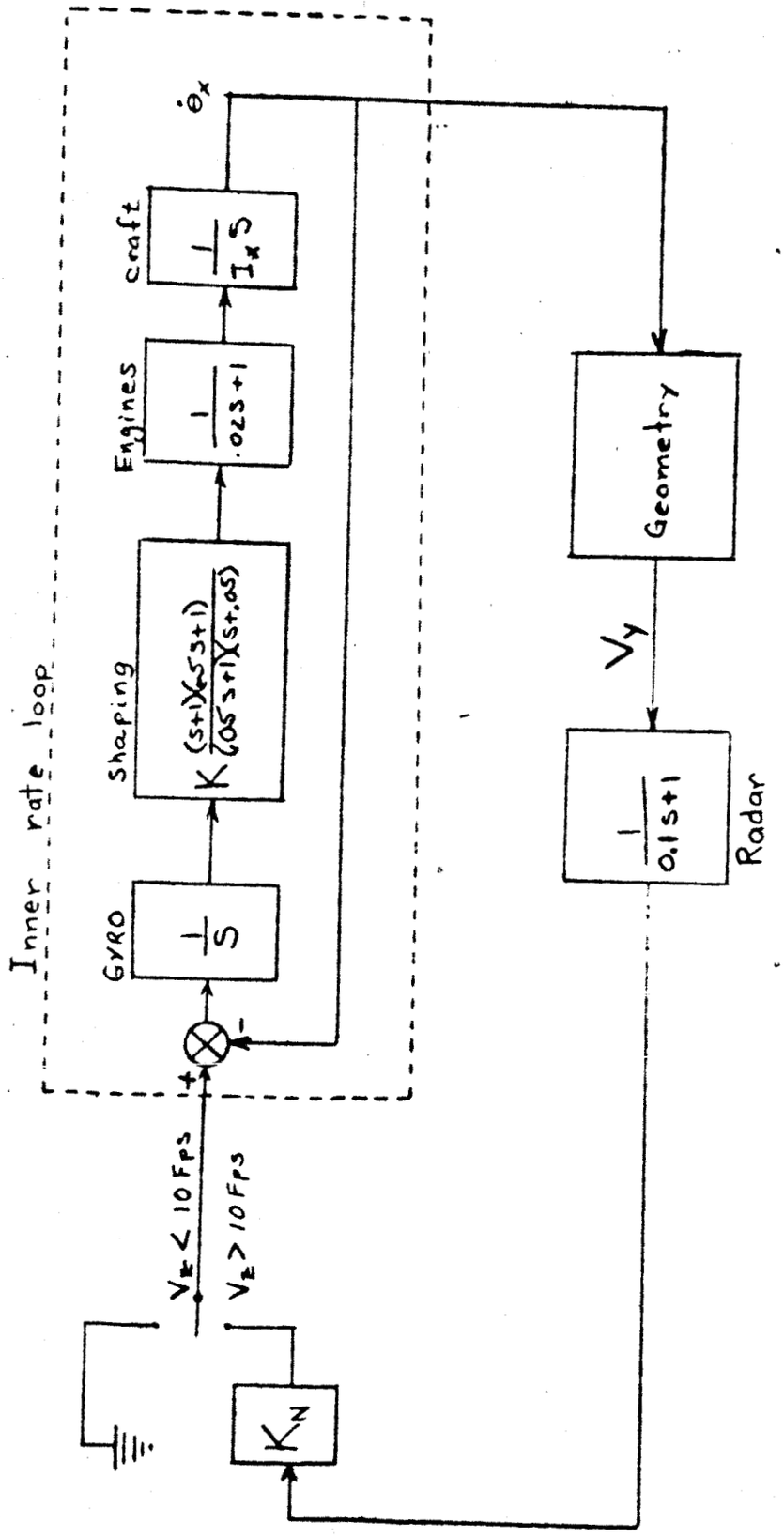

FIGURE 3.6.2 Doppler Attitude Control Loop

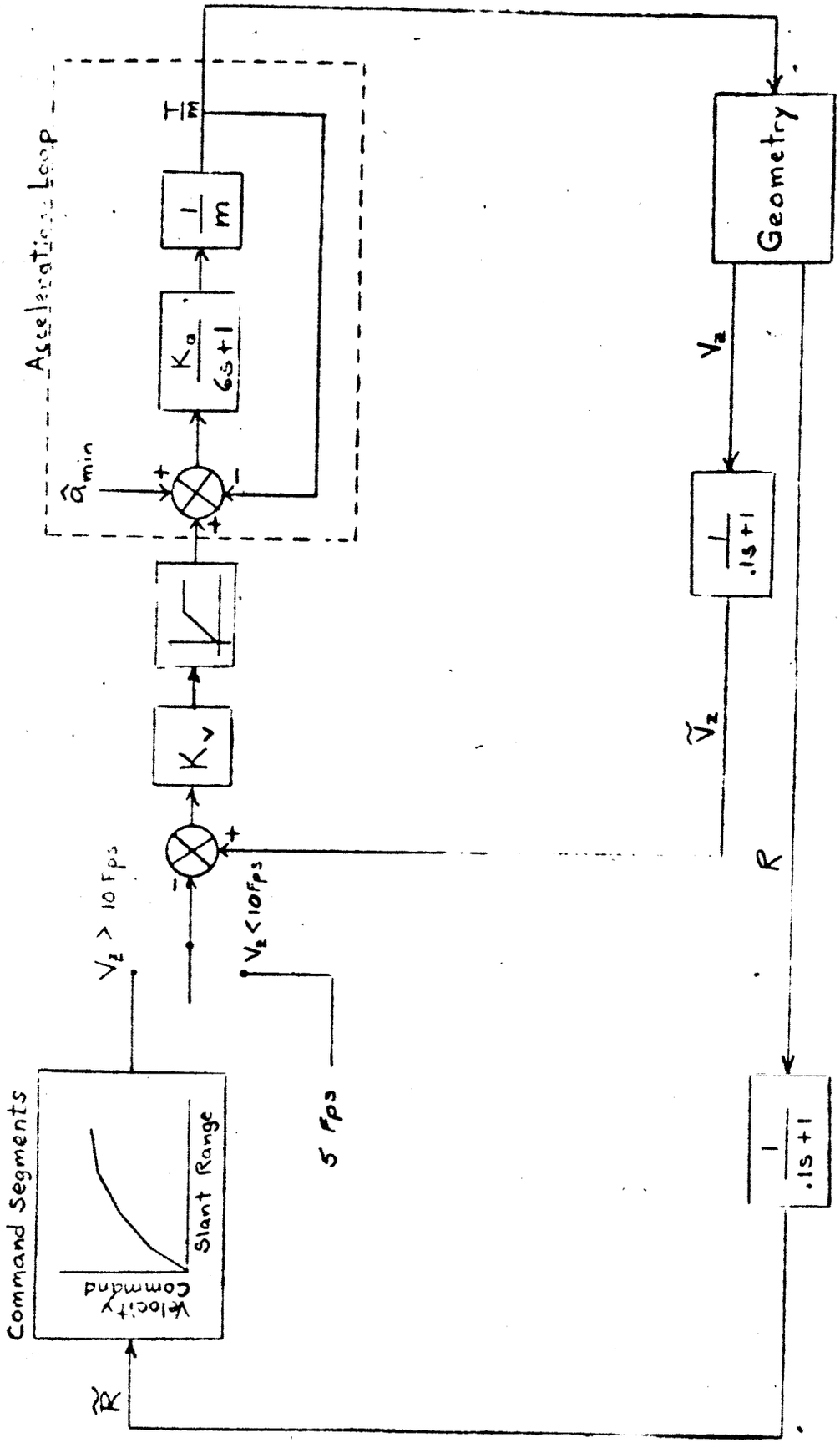

FIGURE 3.6.3 Velocity Control System

4.0 DESIGN CONSIDERATIONS

4.1 Terminal Descent Phase Guidance

4.1.1 Basic Objective: The basic objective of terminal guidance is to effect the transition from the initial conditions listed in Table 4.1.1 to the final conditions listed in Table 4.1.1.

TABLE 4.1.1

Parameter	Initial condition	Final condition
Spacecraft roll axis direction	As desired	Vertical
Velocity vector magnitude	Approximately 8500 fps	5 fps
Velocity vector direction	Either vertical or within 45° of the lunar vertical	Vertical
Slant range to lunar surface	Approximately 55 miles	13 feet

The roll attitude of the spacecraft must be controlled so that a high-gain transmitting antenna is pointed toward Earth.

4.1.2 Description of the Gravity Turn: The method selected to achieve the velocity vector and spacecraft attitude objectives listed in Table 4.1.1 is called the "gravity turn". Under this scheme the spacecraft thrust vector (manually aligned to the roll axis) is continually held in alignment with the velocity vector. If the velocity vector is not vertical, gravity will supply a component of acceleration normal to the velocity vector, and always in a sense which will turn the velocity vector toward the vertical.

4.1.3 Optimum Thrusting Program: Given rocket engines with upper and lower thrust limits, and a fixed range and velocity end point, greatest fuel economy is achieved if the engines operate at minimum thrust as long as possible, and at maximum thrust for the remainder of the thrusting period.

4.1.4 Surveyor Terminal Phase Guidance: Because of certain hardware considerations, the actual terminal descent of the spacecraft is not a gravity turn executed under the optimum throttling program described above. It is not known whether or not the radars will operate properly through the main retrorocket exhaust plume. Since the Doppler Velocity Sensor supplies the steering signals which maintain alignment between the thrust axis and the velocity vector, it is not possible to execute a gravity turn without radars. For these reasons, spacecraft attitude is held fixed during the main retrorocket phase, instead of following a gravity turn.

The optimum throttling program indicates that the engines (main retrorocket and vernier) should not be ignited until the last possible instant and then operated at maximum thrust for the entire descent. Such a throttling program is not feasible because of uncertainties in initial conditions, main retrorocket total impulse, etc. The throttling program actually employed represents a realizable approximation to the theoretically optimum program. Under the instrumented program, the main retrorocket removes the bulk of the spacecraft velocity. At main retrorocket burnout, spacecraft range, velocity, and attitude conditions are such that a gravity turn, executed at maximum vernier engine thrust can achieve the desired cutoff velocity and attitude at a somewhat higher than desired altitude. This higher altitude represents a margin for uncertainties in main retrorocket total impulse, etc. During the vernier phase, a gravity turn is executed under a nearly optimum throttling program.

4.2 Control System Design

4.2.1 Attitude Control

4.2.1.1 Pitch and Yaw Attitude Control

4.2.1.1.1 Inner Rate Loop Design: The description of the considerations which lead to the current inner rate loop design will be carried out by considering the sensor and actuator characteristics, the inputs and disturbances, and the design requirements, and showing how these factors lead to the choice of the shaping amplifier.

The sensor to be employed is a rate integrating gyro. Its output is the integral of the difference between a signal applied to its torquer coil and the spacecraft rate about the pitch (yaw) axis.

The actuator to be employed is the vernier propulsion system. It is capable of producing a moment about the pitch (yaw) axis proportional to the signal out of the shaping amplifier. The vernier propulsion system also introduces a 20 millisecond lag and a hysteresis loop in tandem.

The spacecraft will be considered a rigid inertial sphere with moments of inertia between 115 and 240 slug-feet^2. Thus, the pitch, yaw, and roll loops will be considered inertially uncoupled.

A principal requirement on the inner rate loop is that is accurately maintain the direction of the roll axis in the presence of the disturbance moment generated by main retrorocket thrust vector misalignment. Specifically, it is desired to hold the steady-state pitch (yaw) angle to less than 0.30 degrees in the presence of a disturbance moment of 150 ft-lbs.

Figure 4.2.1 shows a pair of coordinate systems which will be used frequently in succeeding analyses. The xyz coordinate system is the spacecraft body system described in Section 3.1.

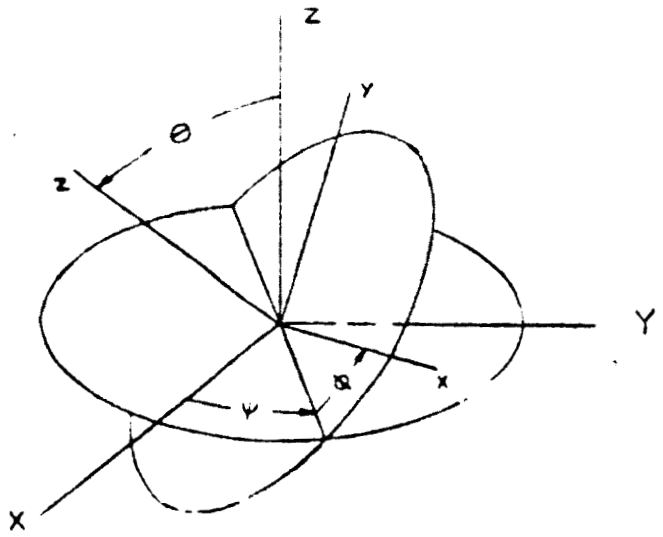

FIGURE 4.2.1

The two systems are related by the Euler angles ψ, φ, θ. The X Y Z coordinate system is an inertially-fixed system defined as follows. For the desired position of the X Y Z system during the main retrorocket phase, $\psi = \varphi = 0$, and $\theta = 90^{\circ}$.

The precise (under the assumption that the spacecraft is an inertial sphere) equations relating spacecraft attitude to total applied moment are as follows:

$$\dot{\vec{\omega}} = \frac{1}{I} \vec{L} \tag{4.2.1}$$

where $\vec{\omega}$ = spacecraft angular velocity vector

I = spacecraft moment of inertia

$\vec{L}$ = total applied moment vector.

$$\dot{\psi} = \frac{1}{\sin \theta} \left[\omega_x \sin \varphi + \omega_y \cos \varphi \right] \tag{4.2.2}$$

$$\dot{\varphi} = \omega_z \frac{\cos \theta}{\sin \theta} \left[\omega_x \sin \varphi + \omega_y \cos \varphi \right] \tag{4.2.3}$$

$$\dot{\theta} = \omega_x \cos \varphi - \omega_y \sin \varphi \tag{4.2.4}$$

where ω_x, ω_y, ω_z are the components of ω in the x, y, z directions respectively. Note that the output signals of the pitch, yaw, and roll gyros are proportional to the time integrals of ω_x, ω_y, and ω_z respectively.

For design purposes, it will be assumed that ψ and φ are small angles, and that the deviation of θ from 90° ($\Delta\theta$) is small. The position of the z-axis for small values of φ, ψ, and $\Delta\theta$ are shown in Figure 4.2.2.

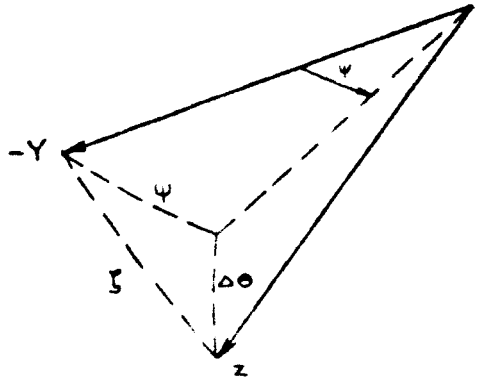

FIGURE 4.2.2

For small ψ and $\Delta\theta$, Figure 4.2.2 indicates that the z-axis pointing error, ζ, is

$$\zeta = \sqrt{\psi^2 + (\Delta\theta)^2} \qquad (4.2.5)$$

Moreover, under the same small angle assumptions, equations (4.2.2) and (4.2.4) become

$$\dot{\psi} \approx \omega_y \qquad (4.2.6)$$

$$\dot{\theta} \approx \omega_x \qquad (4.2.7)$$

Now (4.2.6) and (4.2.7) indicate that for small angles, ψ and θ are nearly equal to the yaw and pitch (respectively) gyro outputs. That is,

$$\theta_x = \theta \qquad (4.2.8)$$

$$\theta_y = \psi \qquad (4.2.9)$$

where θ_x = output of pitch gyro

θ_y = output of yaw gyro

thus, from (4.2.5),

$$\zeta = \sqrt{\theta_x^2 + \theta_y^2} \tag{4.2.10}$$

Also, from (4.2.1), (4.2.6), and (4.2.7),

$$\ddot{\theta}_x = \frac{L_x}{I} \tag{4.2.11}$$

$$\ddot{\theta}_y = \frac{L_y}{I} \tag{4.2.12}$$

As a result of the above considerations, the servo loop diagram of the inner rate loop is as shown in Figure 4.2.3. In this Figure, $K_\theta G_\theta(s)$ is the shaping amplifier transfer function, L_c is the control moment generated by the vernier propulsion system, and L_d is the main retrorocket disturbance moment. An identical diagram

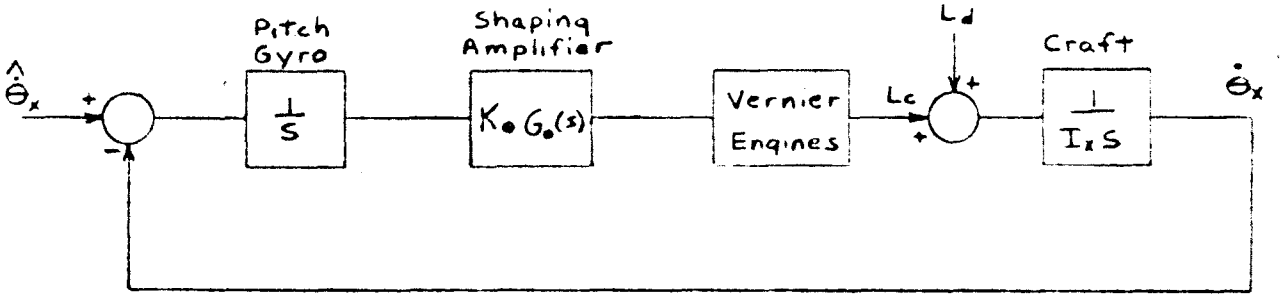

FIGURE 4.2.3

describes the yaw inner rate loop.

Consider now the design of $K_\theta G_\theta(s)$. As a first step consider the question of how many open-loop integrations are desirable (the gyro and geometry supply one each). The inclusion of one integration in $G_\theta(s)$ would provide zero steady-state error in θ_x as a result of L_d. The alternative to an integration is a high value of K_θ. Hardware convenience and noise considerations lead to the choice of including an integration in $G_\theta(s)$.

So far, the S-plane open-loop critical points for the loop shown in Figure 4.2.3 consist of two poles at the origin, one on the real axis at the origin and one at -50. It is clear that stability demands at least two zeros. For hardware convenience these are located on the real axis

to the left of $-\frac{1}{\tau_i}$. Now $G_\theta(s)$ will introduce at least as many poles as zeros. Since two zeros and one pole have been introduced, at least one other pole will appear. This one will be placed to the left of the two zeros. The resulting open-loop pole-zero configuration and the resulting root locus is sketched in Figure 4.2.4.

For purpose of stability, the two zeros should be placed close to the origin, and the pole far from the origin. Two considerations limit the proximity of the zeros to the origin:

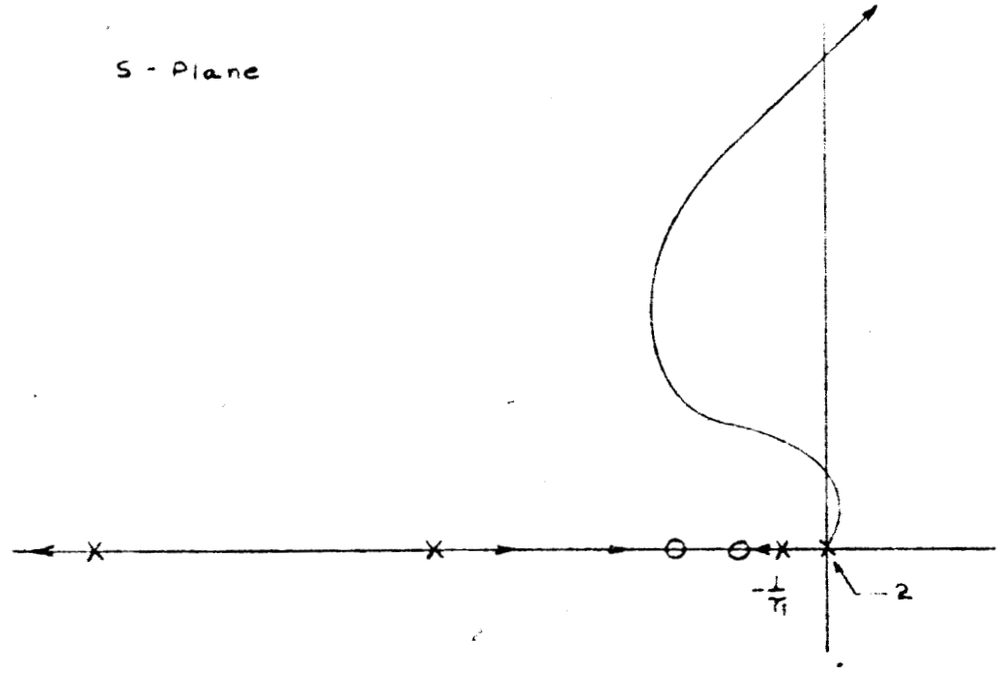

FIGURE 4.2.4

1. As the zeros move closer to the origin, the real root between the zeros and the origin decreases in frequency, and system response becomes correspondingly slower.

2. Capacitor and resistor sizes and tolerances become unwieldy if the zeros are placed too close to the origin. Noise considerations limit placement of the pole too far to the left.

The second of the above considerations governed the selection of the shaping amplifier critical frequency locations. The resulting $G_\theta(s)$ is

$$G_\theta(s) = \frac{(S+1)(0.5S+1)}{S\ .05\ S+1} \qquad (4.2.13)$$

The resulting root locus for the inner rate loop is shown in Figure 4.2.5.

FIGURE 4.2.5

INNER RATE LOOP ROOT LOCUS

LOOP GAIN:

$$\frac{K_\theta}{I}\,\frac{(s+1)(0.5s+1)}{s^2(s+.05)(.05s+1)(.02s+1)}$$

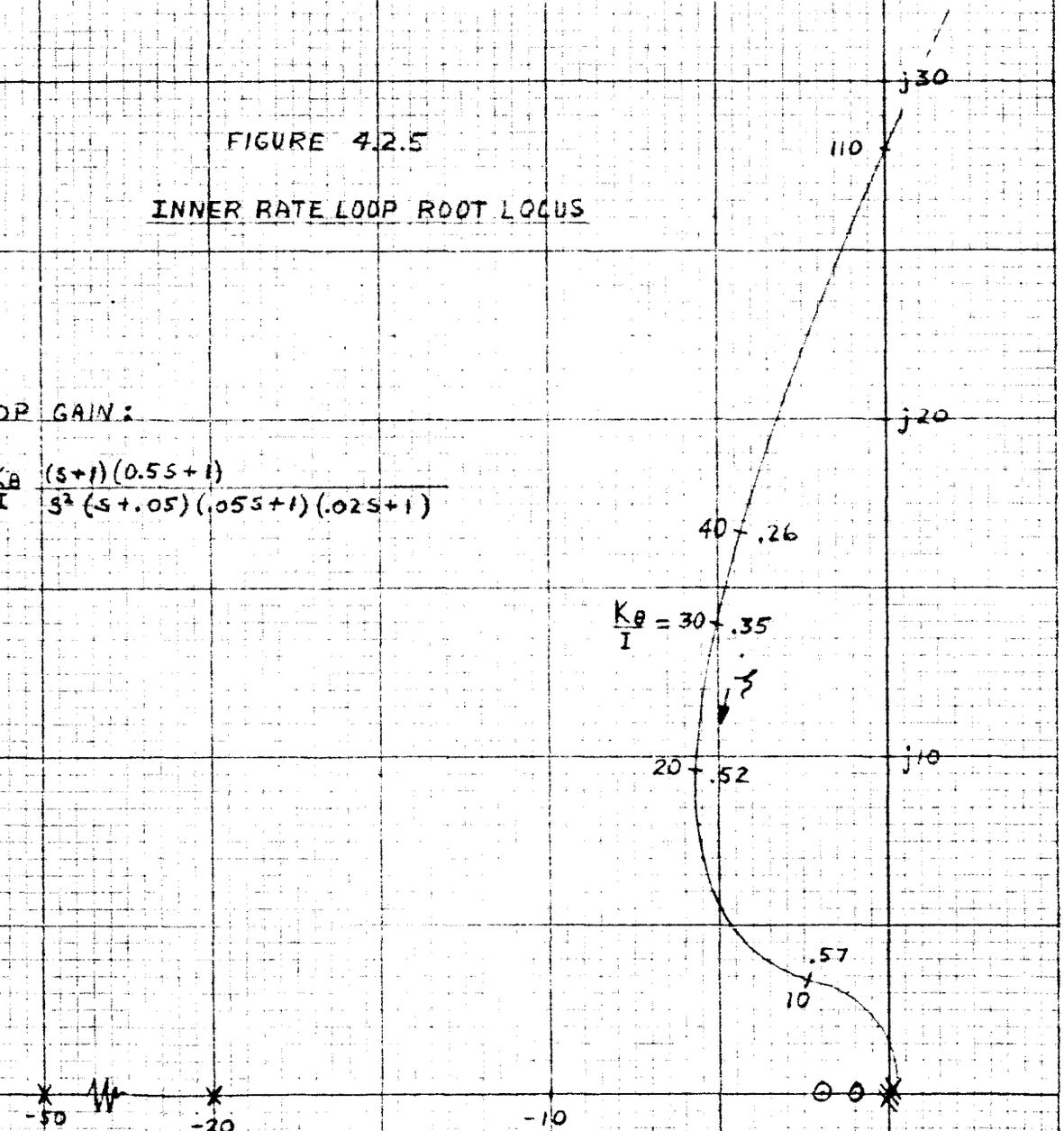

The next step in the inner rate loop design is the selection of a value for K_θ. The selection of this parameter was made on the basis of three considerations:

1. satisfactory stability margins and transient response;
2. steady-state error (in attitude) in the presence of main retrorocket disturbance moment;
3. hysteresis-induced limit cycle amplitude.

The first of these considerations is self-explanatory. The second requires some explanation. On the surface it appears that steady-state error in the presence of L_d should be zero. If the electronic integrator contained in the shaping amplifier were a perfect integrator this would be so. In fact, however, the electronic "integrator" is more accurately described as a first order lag with a relatively long time constant, τ_i. The longest time constant conveniently available was 20 seconds. The resulting $G_\theta(s)$, then is

$$G_\theta(s) = \frac{(S + 1)(0.5\ S + 1)}{(S + .05)(.05\ S + 1)} \qquad (4.2.14)$$

and the steady-state error, θ_{xe}, in pitch (yaw) error is

$$\theta_{xe} = \frac{.05}{K_\theta} L_d \qquad (4.2.15)$$

The third of the above considerations, which turned out to be the governing one, is discussed in detail in Reference 3. This work will now be briefly summarized. A quantative estimate (and, as analog simulation later confirmed, a very good one) of limit cycle behavior was made by means of a describing function analysis. Figure 4.2.6 shows a plot of the linear portion of the open-loop transfer function

$$G(j\omega) = \frac{K_\theta}{I} \frac{(j\omega + 1)(0.5\ j\omega + 1)}{S^2(j\omega + .05)(.05j\omega + 1)} \qquad (4.2.16)$$

for several values of $\frac{K_\theta}{2}$, and the negative inverse of the describing function, $N\left(\frac{H}{M}\right)$. H is the hysteresis width, (see Figure 4.2.7) and M and N are defined as follows. If the input to the hysteresis is $Me^{j\omega t}$, the output is $N\,M\,e^{j\omega t}$ $+ \sum_{n=2}^{\infty} \left[A_n e^{nj\omega t} + A_{-n} e^{-nj\omega t}\right]$, where M is real and M and the A_n are,

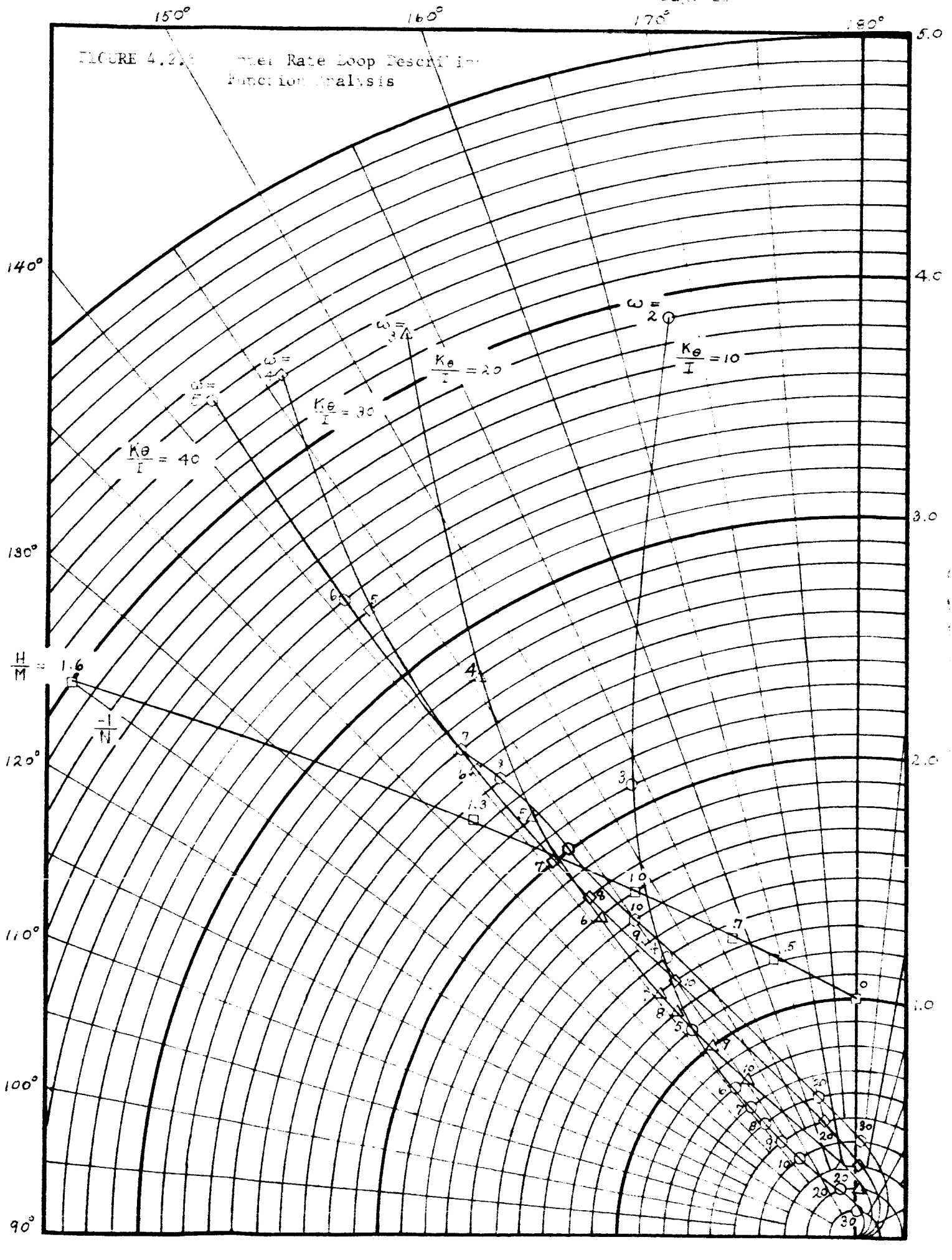
150°
160°
170°
180°
140°
130°
120°
110°
100°
90°
5.0
4.0
3.0
2.0
1.0
$\frac{K\theta}{I} = 10$
$\frac{K\theta}{I} = 20$
$\frac{K\theta}{I} = 30$
$\frac{K\theta}{I} = 40$
$\omega = 2$
$\omega = 3$
$\omega = 4$
$\omega = 5$
$\frac{H}{M} = 1.6$
$\frac{-1}{N}$

in general, complex. Describing function theory concludes that the amplitude and frequency of the limit cycle (at the input to the hysteresis) are those corresponding to the intersection of $G(j\omega)$ and $-\frac{1}{N}$. The variable of interest is $\textcircled{H}$, the amplitude of the limit cycle, two integrations downstream from the hysteresis output,

$$\textcircled{H} = \frac{|N|M}{I\omega^2} \tag{4.2.17}$$

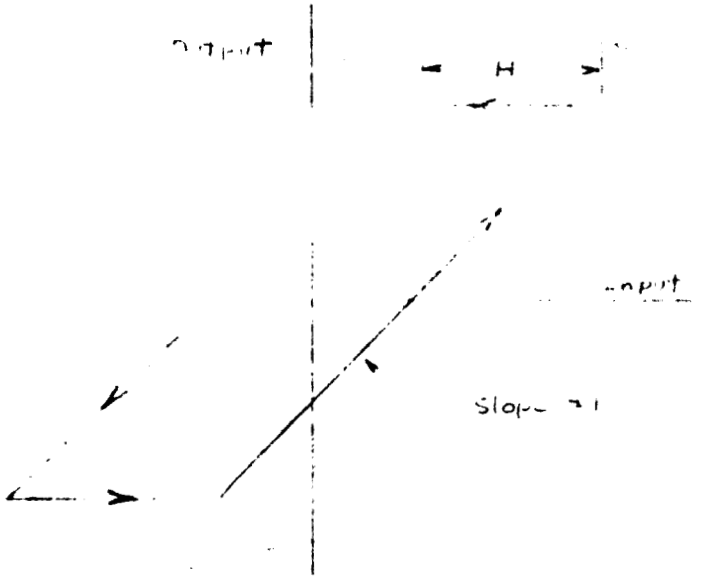

FIGURE 4.2.7 Hysteresis Characteristic

Since the describing function is plotted as a function of $\frac{H}{M}$, and H and I are constants, it is helpful to rewrite (4.2.17) as

$$\textcircled{H} = \frac{H}{I} \frac{|N|}{\left(\frac{H}{M}\right)\omega^2} \tag{4.2.18}$$

It is clear from Figure 4.2.6 that as $K_{\theta/I}$ increases from 10 to 40, the values of N, $\left(\frac{H}{M}\right)$ and ω vary as follows:

$|N|$ decreases until $\frac{K_\theta}{I} \approx 30$, and then increases; $\left(\frac{H}{M}\right)$ increases until $\frac{K_\theta}{I} \approx 30$, and then decreases; ω increases over the entire range. This behavior indicates the possibility of an optimum value of $K_{\theta/I}$. It turns out that if such a peak exists, it is beyond $K_{\theta/I} = 30$. For values of gain in this range, transient performance becomes a controlling consideration. Figure 4.2.8 shows plots of inner rate loop damping factor, ζ, and

FIGURE 4.2.8

INNER RATE LOOP DAMPING RATIO
AND LIMIT CYCLE AMPLITUDE
VS. LOOP GAIN CONSTANT

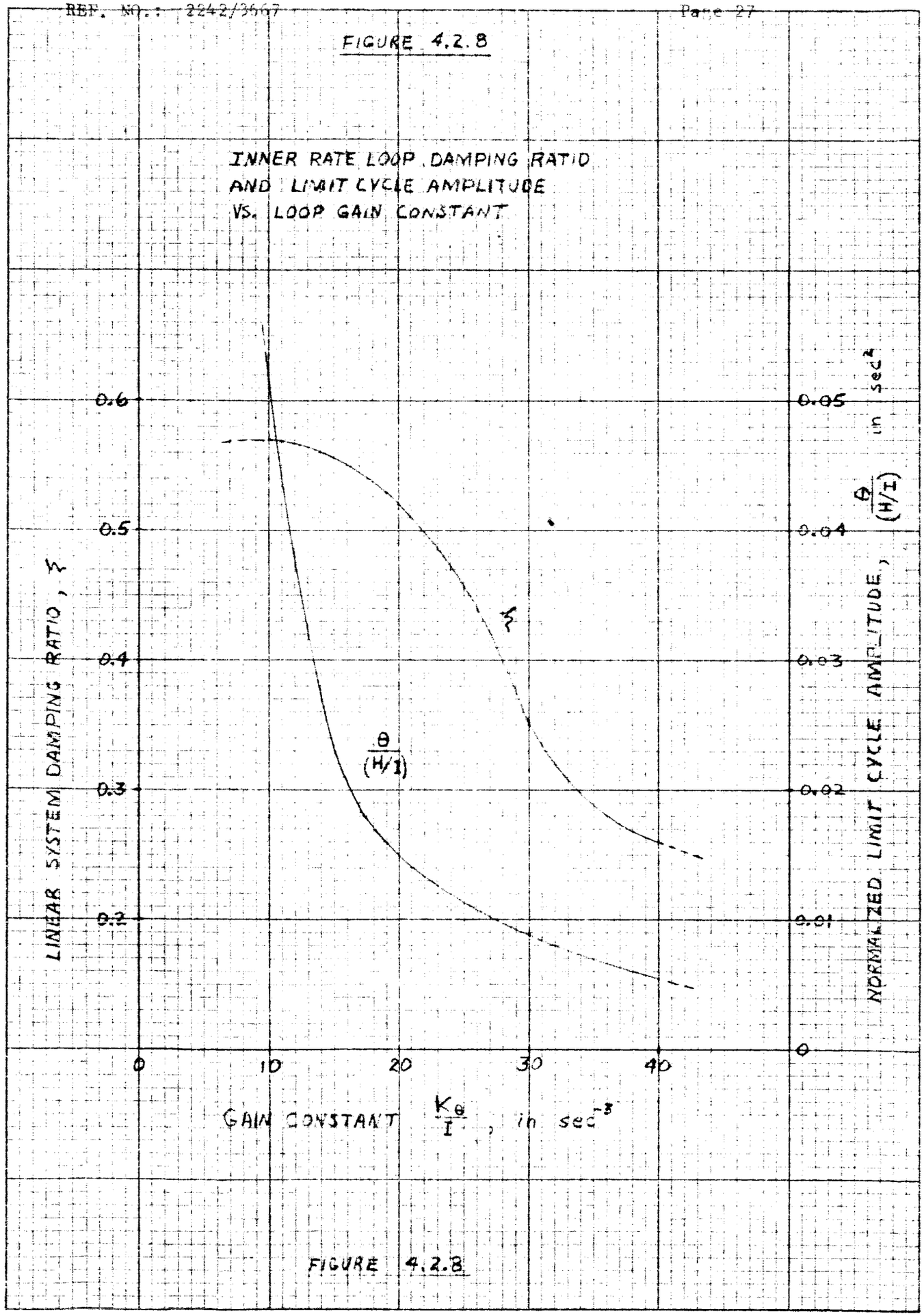

FIGURE 4.2.8

limit cycle amplitude, (H), versus $K_{\theta/I}$. As a reasonable compromise between limit cycle amplitude considerations, and transient response and stability considerations, a value of $K_{\theta/I}$ of 27 was chosen. A value of $I = 160$ slug-ft^2, which represents the mean between the predicted mission extremes of 200 and 120 slug-ft^2, was used to compute the value.

$$K_\theta = 4.32 \times 10^3 \text{ lb-ft/sec/rad} \qquad (4.2.19)$$

Next, consider the steady-state error in attitude in the presence of the main retrorocket disturbance moment. If it is assumed that the magnitude of the disturbance moment vector is 150 lb-ft, and that it is directed along the pitch axis, then equation (4.2.15) yields

$$\theta_{xe} = \frac{.05}{4.32 \times 10^3} (150) = 1.735 \times 10^{-3} \text{ radian}$$

or

$$\theta_{xe} = 0.1 \text{ degree}$$

which is well within the target figure set earlier.

4.2.1.1.2 Doppler Attitude Loop. There are two parameters in the Doppler attitude loop, which must be chosen (see Figure 3.6.2):

1. The limiter saturation value;
2. The Doppler amplifier gain, K_N.

The purpose of the limiter is to prevent large initial flight path angles from causing the gyros to bang their stop and possibly set up an unstable motion. The value of 5.5°/sec. was chosen as the smallest value consistent with the requirement that flight path angle be nulled within 9 seconds from an initial value of 45° (see sections 3.10.2.1 of Reference 4.). The 5.5°/sec number is also called-out directly in section 4.3.5 of Reference 4.

The gain, K_N, was chosen purely on the basis of stability and hardware convenience. The stability analysis will be carried out by considering a planar small angle model. Figure 4.2.9 shows the geometry of this model. In this figure, ℓ and v are inertial reference axes,

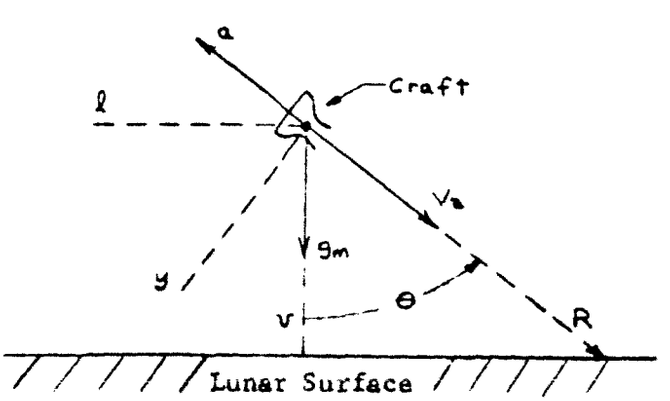

Figure 4.2.9

g_m is the gravity vector, y and z are the spacecraft axes, V_z is the velocity and a is the acceleration resulting from the vernier propulsion system thrust. Equations of motion for this model are

$$\dot{V}_\ell = a \sin \theta \tag{4.2.20}$$

$$\dot{V}_v = g_m - a_{cos}\ \theta \tag{4.2.21}$$

$$V_y = V_\ell \cos \theta + V_v \sin \theta \tag{4.2.22}$$

where V_ℓ and V_v are the components of the velocity vector along the respective axes.

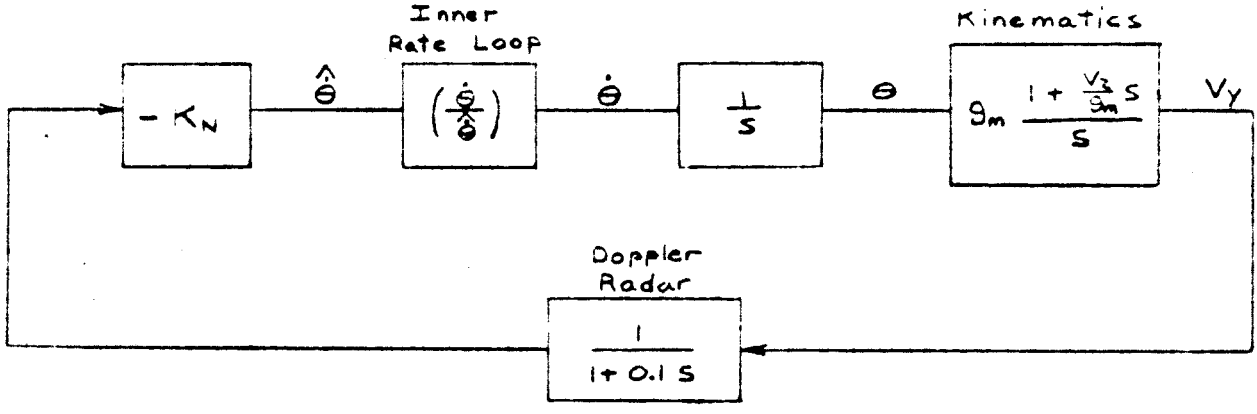

FIGURE 4.2.10 Doppler Attitude Loop

According to (4.2.22), $\dot{V}_y$ is

$$\dot{V}_y = \dot{V}_\ell \cos \theta + \dot{V}_v \sin \theta - V_\ell \dot{\theta} \sin \theta + V_v \dot{\theta} \cos \theta \tag{4.2.23}$$

or, substituting from (4.2.20) and (4.2.21):

$$\dot{V}_y = g_m \sin \theta + \dot{\theta} (V_v \cos \theta - V_\ell \sin \theta) \tag{4.2.24}$$

But $V_v \cos \theta - V_\ell \sin \theta = V_z$ (4.2.25)

so that (4.2.24) becomes

$$\dot{V}_y = g_m \sin \theta + \dot{\theta} V_z \tag{4.2.26}$$

For small values of θ, (4.2.26) may be written

$$\dot{V}_y = g_m \theta + \dot{\theta} V_z \qquad (4.2.27)$$

Now if V_z is constant or varying slowly, (4.2.27) may be written in Laplace notation as

$$V_y = \frac{V_z \left(S + \frac{g_m}{V_z}\right)\theta}{S} \qquad (4.2.28)$$

Thus, by using equation (4.2.28) in the "geometry" box in Figure 3.6.2, the Doppler attitude loop may be represented as shown in Figure 4.2.10. The stability analysis of this loop will now be discussed.

The open-loop critical frequencies of the Doppler loop (Figure 4.2.10) consist of the following:

1. The closed-loop critical frequencies of the inner rate loop;
2. Two integrations and a zero at $S = -\frac{g_m}{V_z}$ from the geometry;
3. A pole at S = -10 from the radar.

The open-loop gain is $K_N g_m$. The design procedure is carried out as follows:

1. Plot the root locus for V_z = 700 fps (the maximum velocity at which the loop operates) with K_N as the parameter and set K_N to provide reasonable stability margins and transient performance.
2. Plot the root locus with K_N equal to the value chosen in step 1 and V_z as the parameter. Use this locus to determine the point at which transient performance or stability margin has deteriorated to an unacceptable point.
3. Repeat step 1 using for V_z the value found in step 2.
4. Using for K_N the value found in step 3, repeat step 2 to insure adequate performance down to V_z = 10 fps.

The root locus called for by step 1 is shown in Figures 4.2.11 and 4.2.12. Observe that the roots shown in Figure 4.2.11 tend to the right with increasing gain, while those of Figure 4.2.12 tend to the left. Since the zero located at

$S = -\frac{g_m}{V_z}$ does not change position much for V_z above 50 fps, and

the open-loop gain is $K_N V_z$, the roots will vary with V_z in about the same fashion they do with K_N for a wide range of V_z. Since V_z will decrease from 700 feet per second, K_N should be set as high as possible to enhance stability margin for the roots of Figure 4.2.12 at lower velocity. The roots of Figure 4.2.11, however, prohibit excessive values of K_N. The highest value of K_N compatible with both the roots of Figure 4.2.12 and hardware convenience is

$$K_N = 2.8 \times 10^{-3} \text{ radians/foot} \qquad (4.2.29)$$

This is the value selected for use above the 1000 foot mark.

The locus called for in step 2 is shown in Figures 4.2.13 and 4.2.14. Since the roots shown in Figure 4.2.14 are satisfactory around 100 feet/second, it was decided to alter the value K_N on signal from the already-available 1000 foot range mark (which occurs at around 100 feet per second).

The root locus called for in step 3 is shown in Figures 4.2.15 and 4.2.16. The value of K_N chosen for use below the 1000 foot mark is

$$K_N = 1.7 \times 10^{-2} \text{ radians/foot} \qquad (4.2.30)$$

The root locus called for in step 4 is shown in Figures 4.2.17 and 4.2.18. These figures show that performance should be satisfactory down to 10 fps, where the Doppler attitude loop is opened.

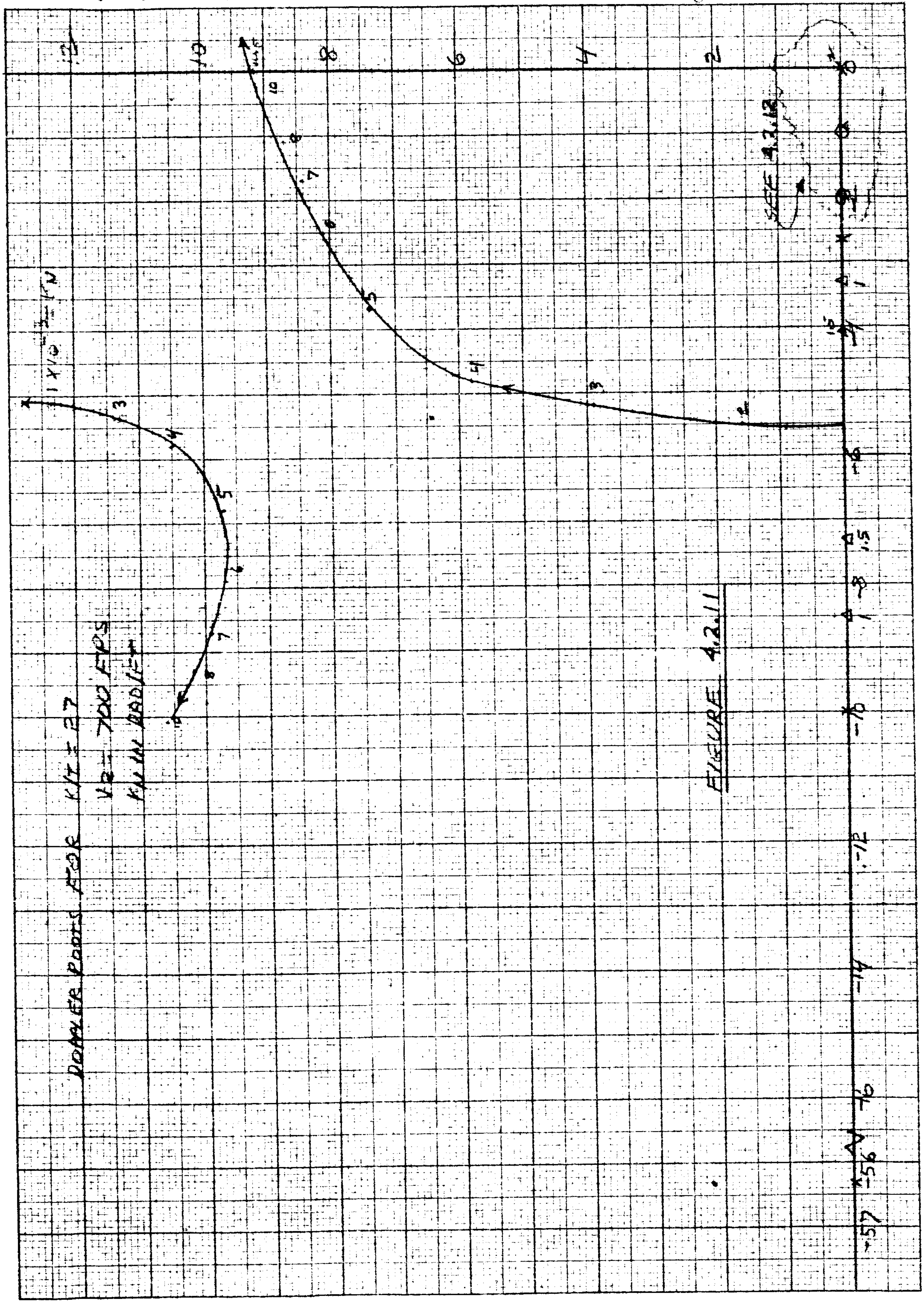
DOPPLER ROOTS FOR K/T = 27
VR = 700 FPS
K = 1N RAD/FT
SEE 4.2.12
FIGURE 4.2.11

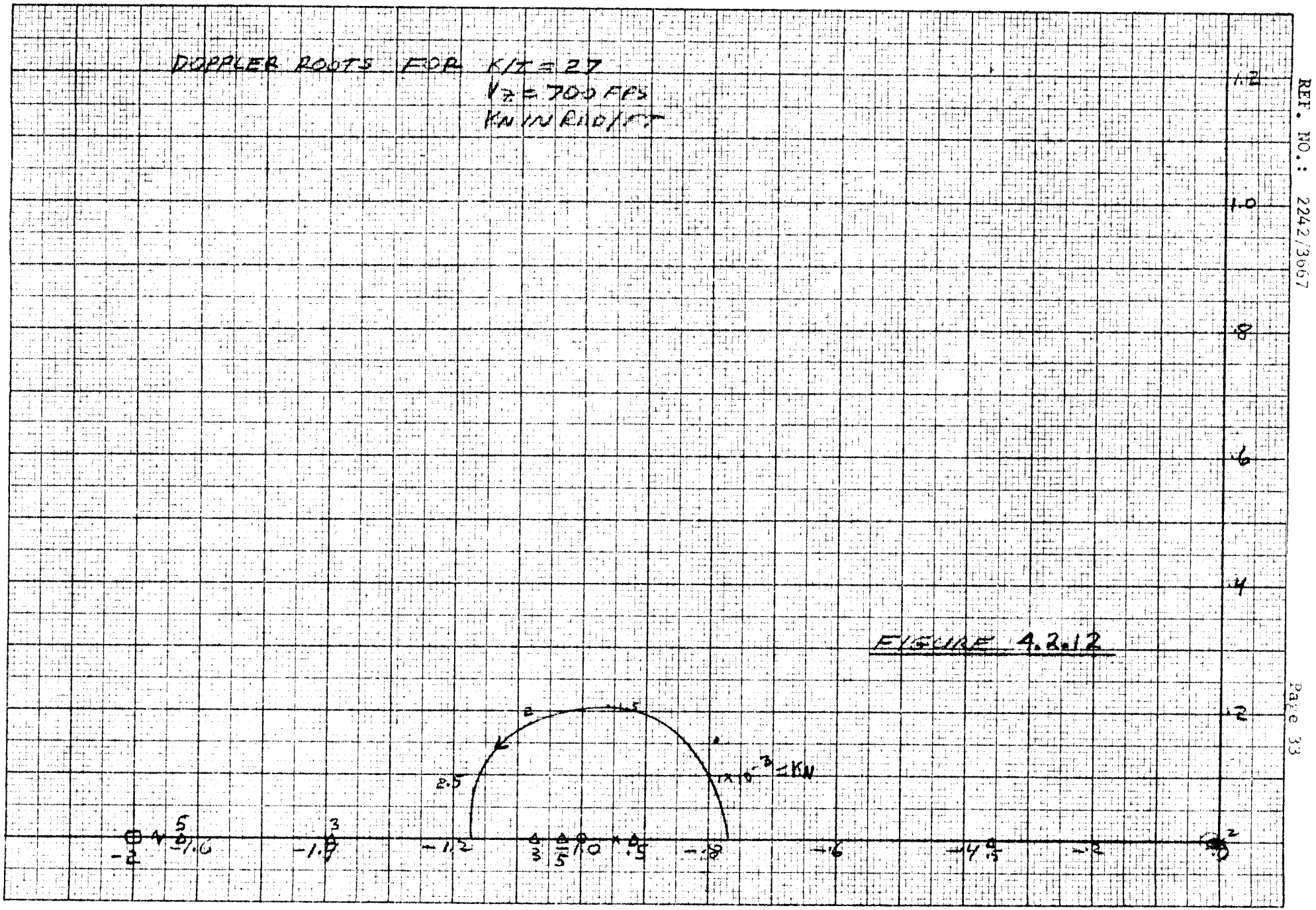

FIGURE 4.2.12

DOPPLER POLES FOR $K_N = 2.8 \times 10^{-3}$

$K/\epsilon = 2.7$

V_2 IN FPS

FIGURE 4.2.13

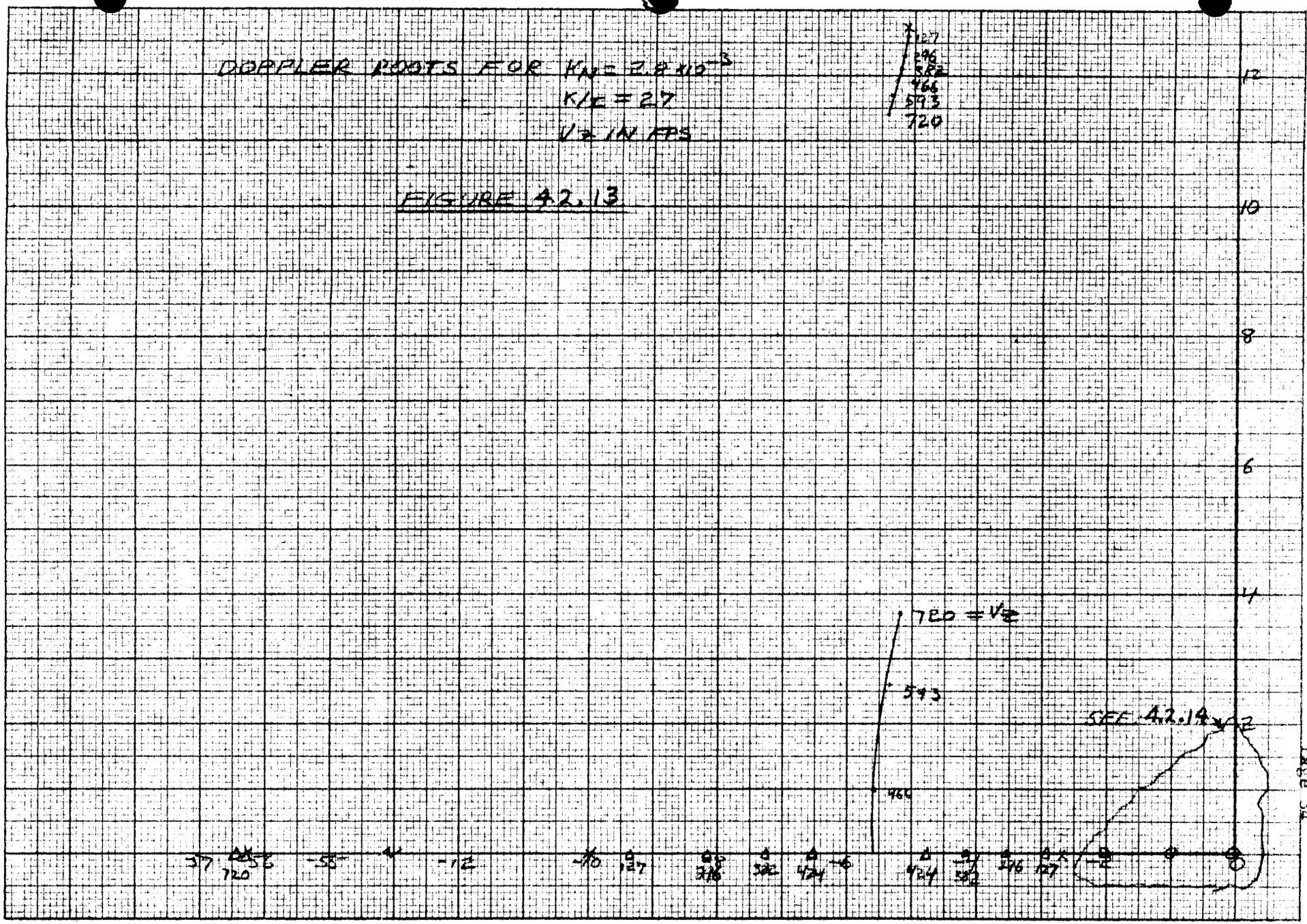

DOPPLER ROOTS FOR $M_N = 2.8 \times 10^{-3}$
$K/L = 27$
V_2 IN FPS

FIGURE 4.2.14

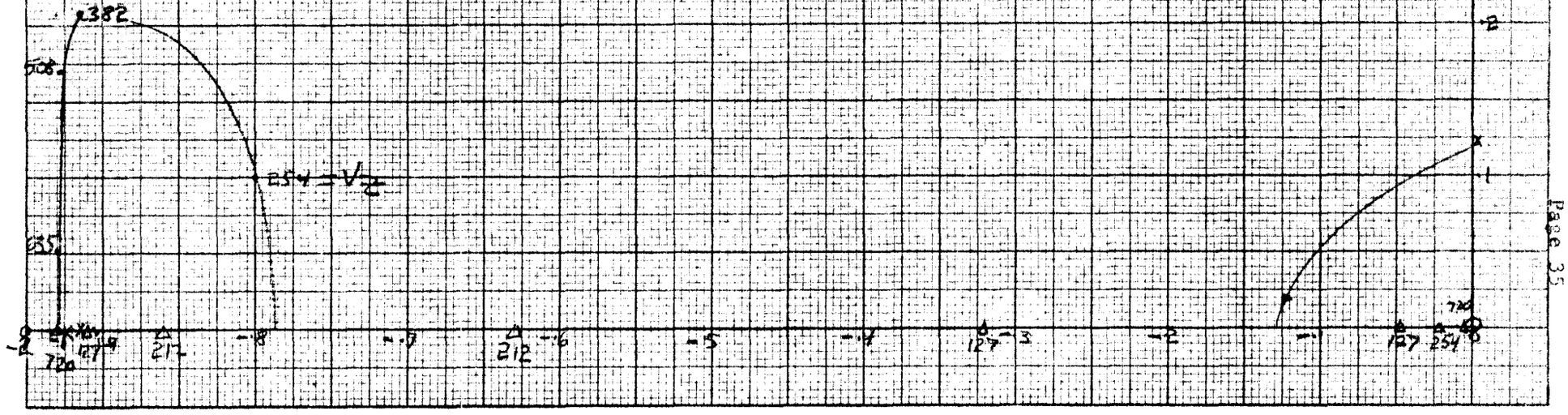

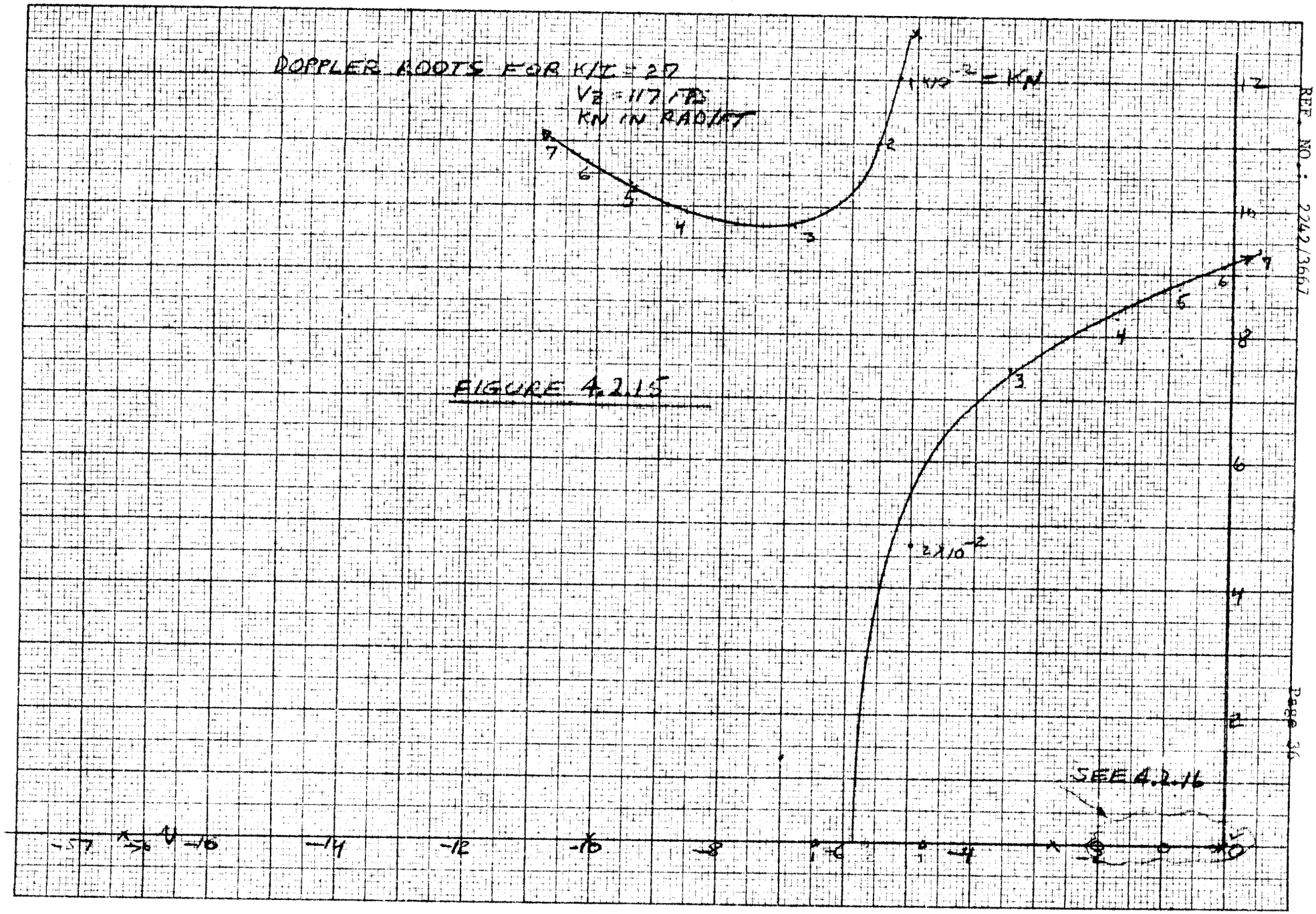

FIGURE 4.2.15

DOPPLER ROOTS FOR K/E = 2.7
V2 117 CPS
KN IN RADIET

FIGURE 4.2.16

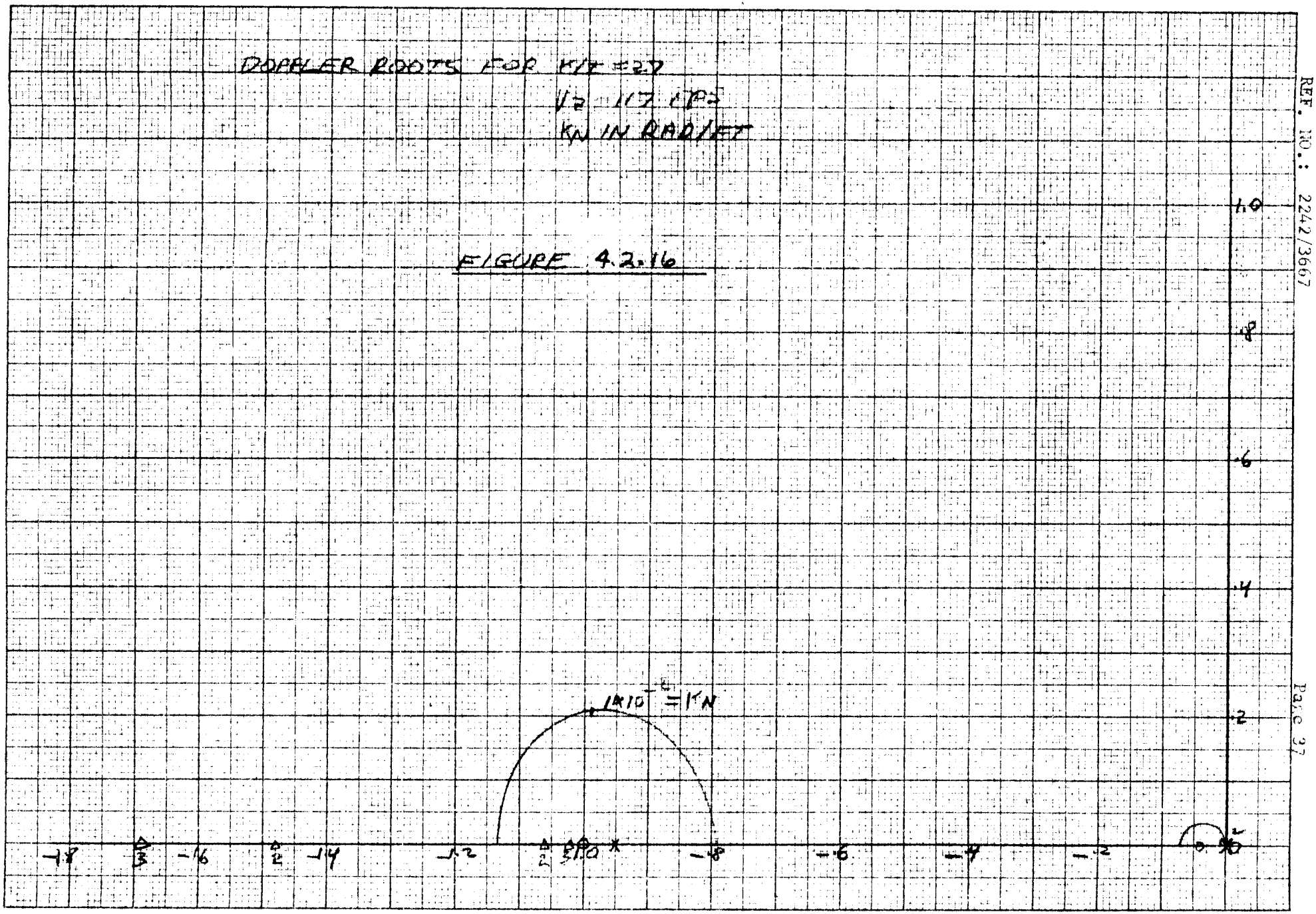

DOPPLER ROOTS FOR $K_N = 1.7 \times 10^{-3}$
$K/I = 27$
V_z IN FPS

FIGURE 4.2.18

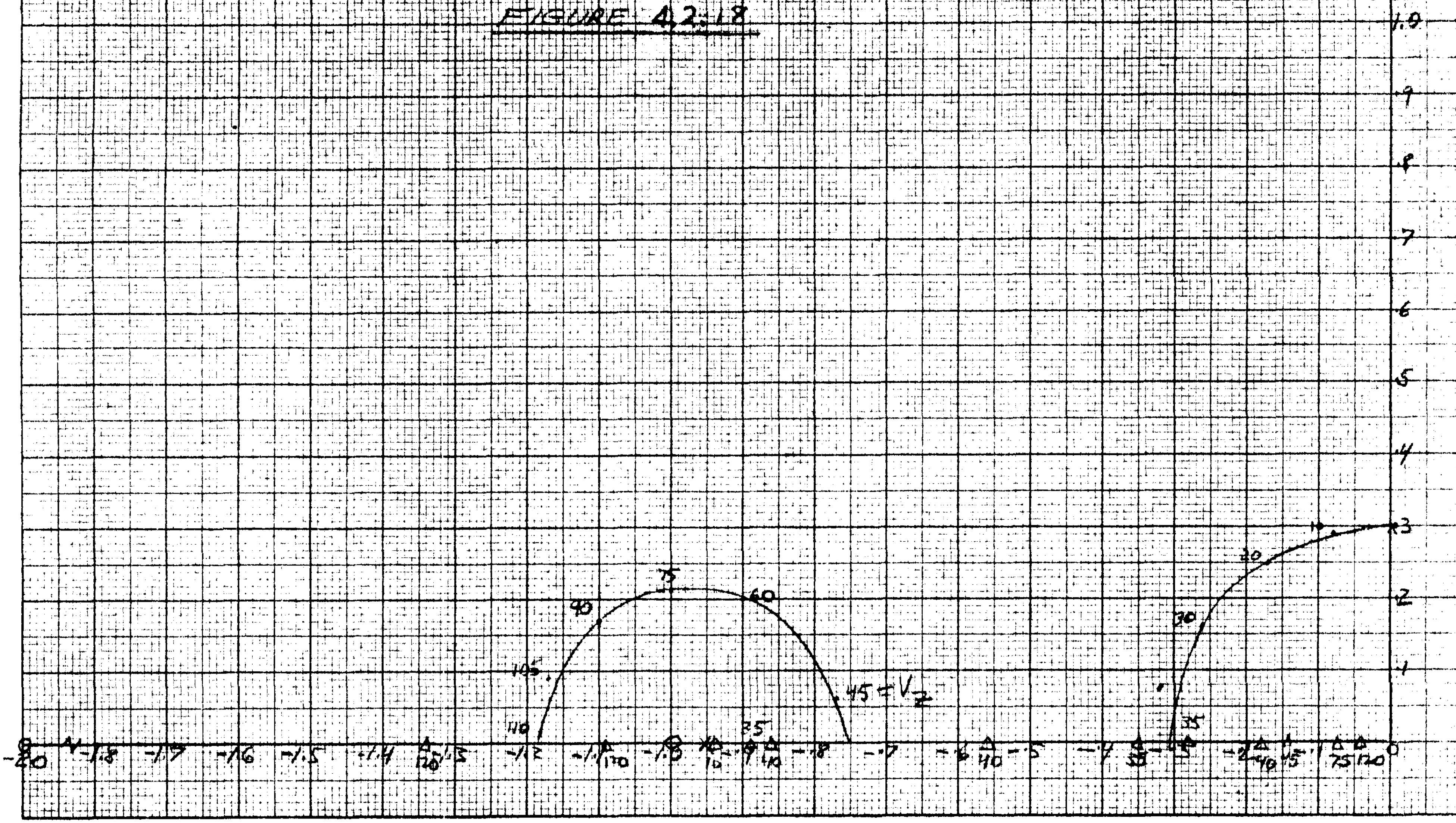

4.2.2 Thrust Control

4.2.2.1 Acceleration Loop. The purpose of the acceleration loop is to control the vernier engine thrust to a precision thrust-to-mass ratio. The loop configuration is shown in Figure 4.2.19. The chief considerations here

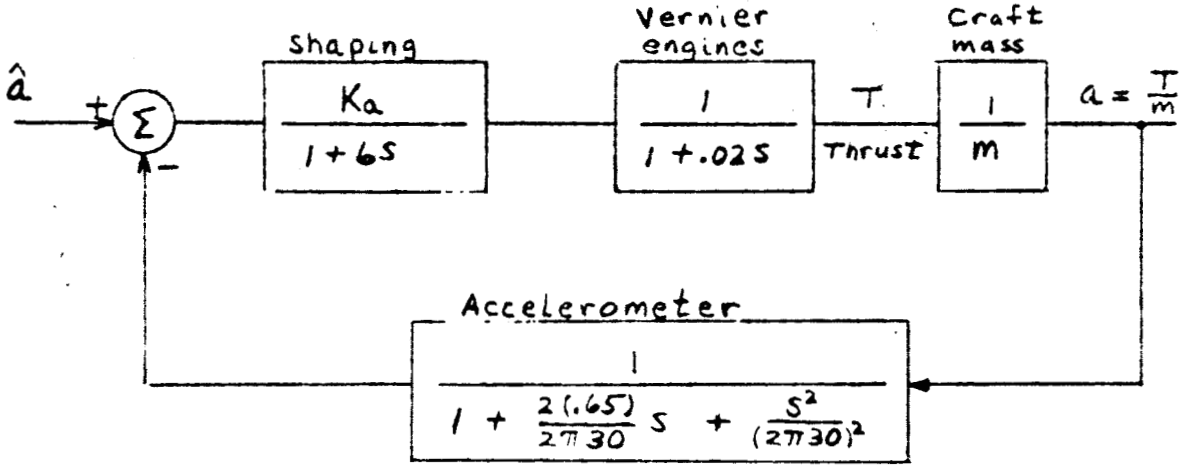

FIGURE 4.2.19 Acceleration Loop

are low steady-state error, response fast enough to keep total impulse errors low (during the midcourse velocity correction) but slow enough to avoid elastic modes, and reasonable damping and stability margins. These considerations are discussed in more detail in Reference 5.

The pole-zero configuration of the acceleration loop without compensation is sketched in Figure 4.2.20. Note that high values of gain tend to drive

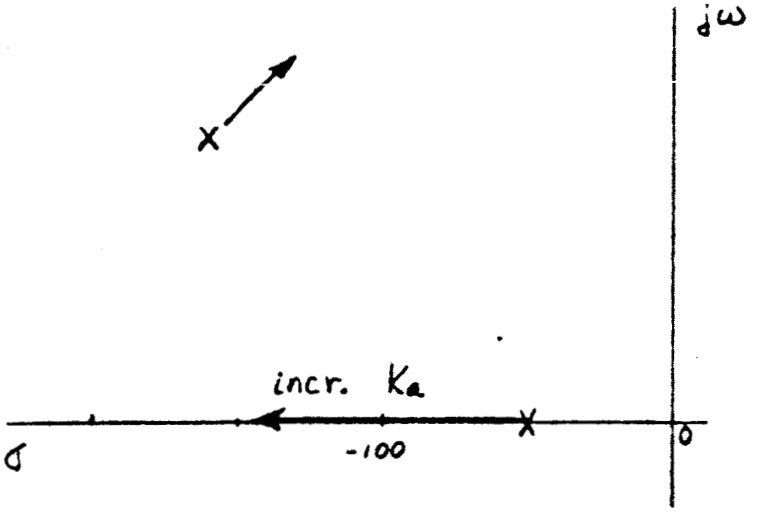

FIGURE 4.2.20

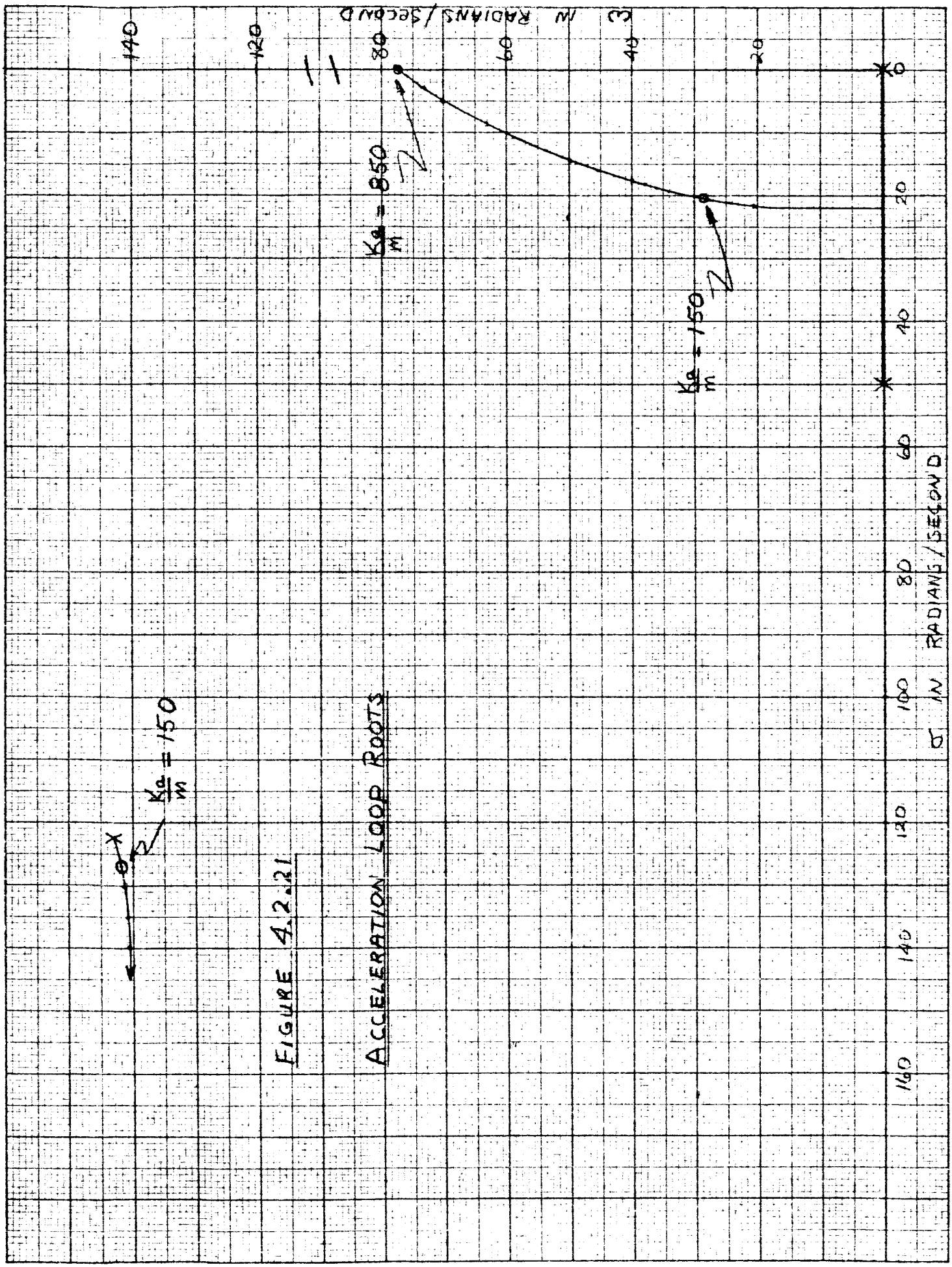

FIGURE 4.2.21

ACCELERATION LOOP ROOTS

the root emanating from the engine pole to an objectionably high frequency. In order to prevent this, the loop is compensated by

$$G(s) = \frac{1}{6S + 1} \tag{4.2.31}$$

the root locus for the compensated loop is shown in Figure 4.2.21. The value of K_a chosen is

$$K_a = 2240 \ \frac{\text{lb-ft}}{\text{sec}^2} \tag{4.2.32}$$

the expected range of K_a/M, then is

$$34 < \frac{K_a}{m} < 120 \ \text{ft/sec}^2 \tag{4.2.33}$$

where m is spacecraft mass. Figure 4.2.21 indicates satisfactory performance in this range.

4.2.2.2 Velocity Loop. The configuration of the velocity loop is shown in Figure 4.2.2.2 The geometry used in this discussion and that on the range loop was shown in Figure 4.2.9. For purposes of range, acceleration, and

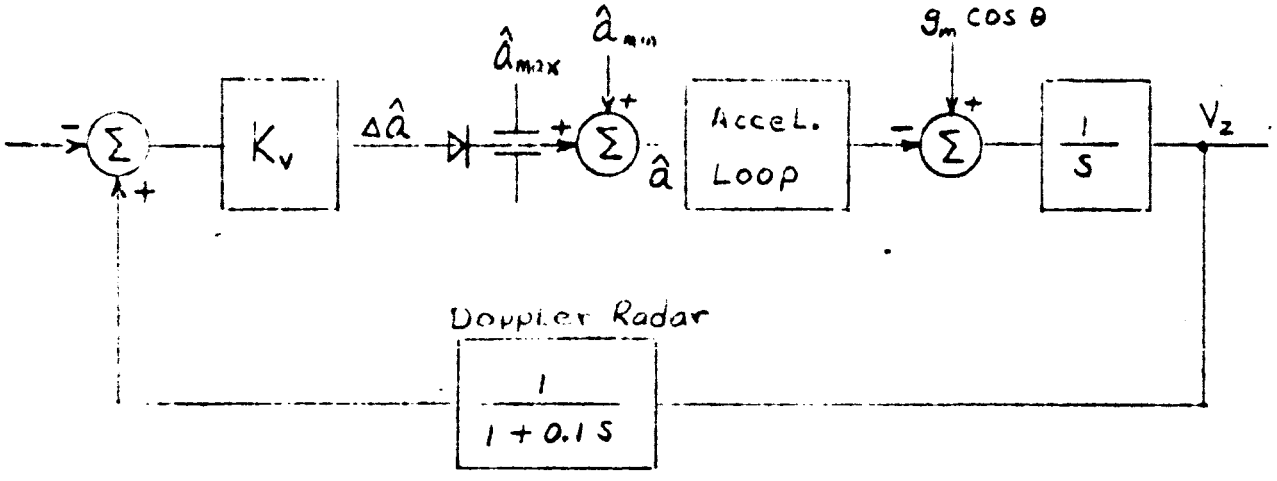

FIGURE 4.2.22 Velocity Loop

velocity loop design, θ will be assumed small.

It is assumed that the Doppler attitude loop maintains perfect alignment between the velocity vector, V, and the z-axis. Slant range, R, is the distance from the spacecraft to the lunar surface measured in the direction of the z-axis, and g_m is the lunar gravity vector.

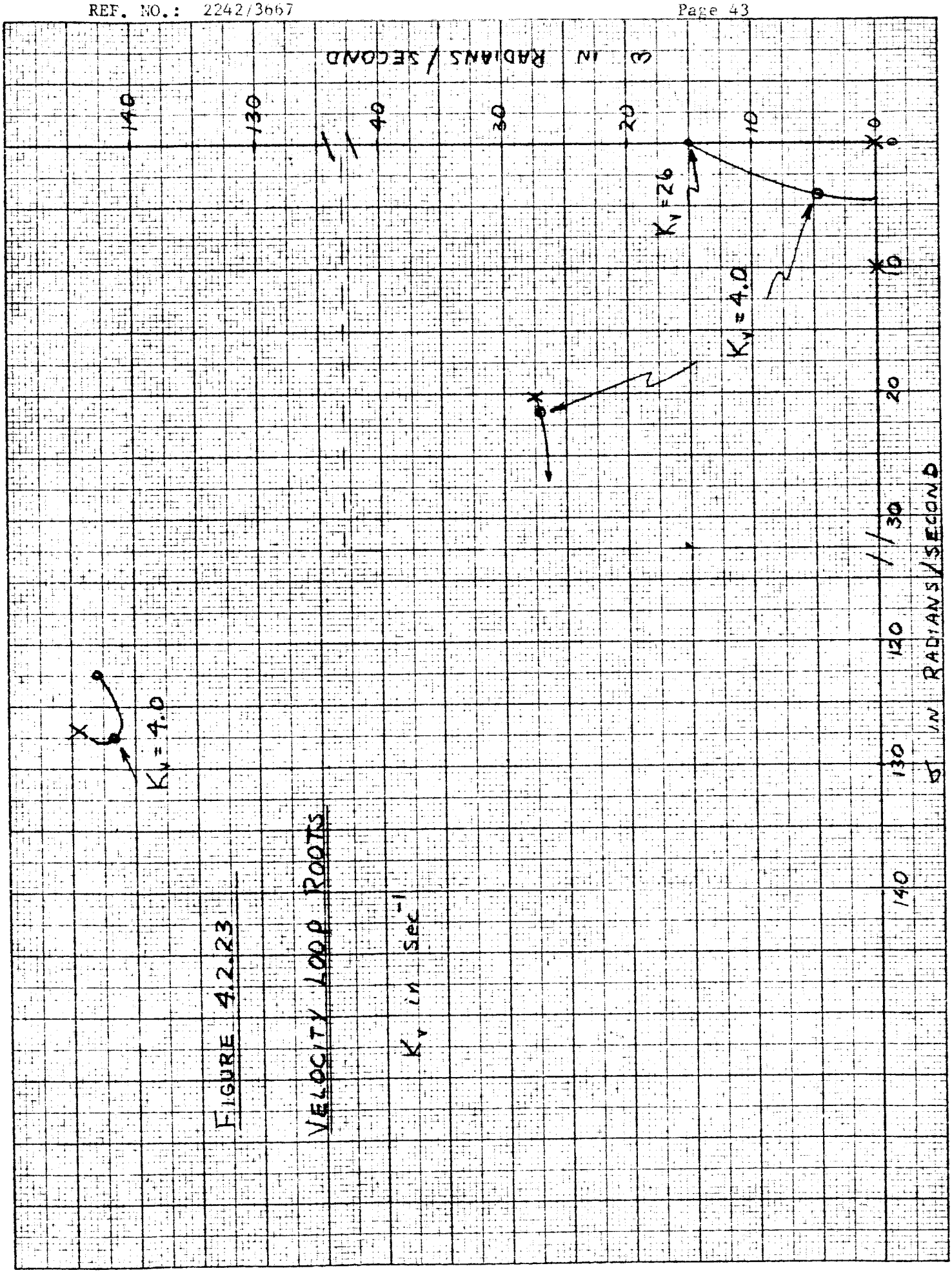

FIGURE 4.2.23

VELOCITY LOOP ROOTS

K_v in Sec^{-1}

The linear design of this loop is straightforward. The root locus for the loop is shown in Figure 4.2.23. On the basis of this root locus, a value of

$$K_v = 4 \text{ sec}^{-1} \tag{4.2.34}$$

was chosen.

A limiter and a bias, $\hat{a}_{min}$, are located between the descent amplifier and the acceleration loop. The net characteristic of limiter and bias are as shown in Figure 4.2.24. The limits, $\hat{a}_{min}$ and $\hat{a}_{max}$,

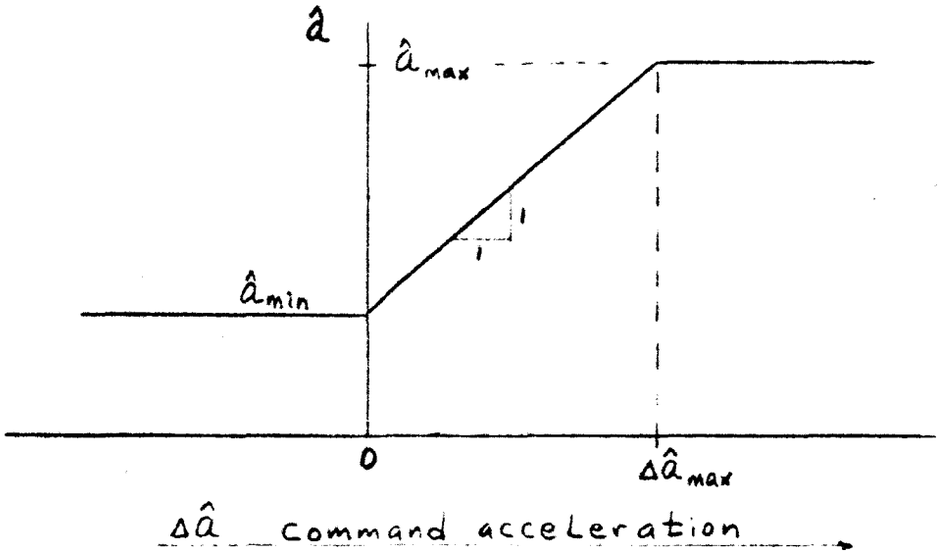

FIGURE 4.2.24 Acceleration Command Limit and Bias Characteristic

are chosen so that a linear portion of the vernier engine thrust range is reserved for moment control during the vernier descent phase. These values are chosen as follows.

If the moment arms (thrust vector to spacecraft center of gravity) for each vernier engine were equal, the differential throttling command from the pitch and yaw rate loops would be zero, and the full throttling range of 30 to 104 pounds per engine would be available. Because of unavoidable mechanical tolerances, these moment arms are not equal. The net result of the tolerances is that the spacecraft center of gravity is located on a circle of radius 1.03 inches (see Reference 6) centered on the geometric center of the three engines. This is shown in Figure 4.2.25. In the steady-state, the inner rate loops will throttle the three engines so that the pitch and yaw moments about the spacecraft center of gravity are zero. The total thrust will be throttled to some value T by the acceleration loop. These conditions are expressed as follows:

$$L_{x'} = 0 = -r_1 T_1 \cos \theta_1 + r_2 T_2 \sin \theta_2 + r_3 T_3 \sin \theta_3 \quad (4.2.35)$$

$$L_{y'} = 0 = -r_1 T_1 \sin \theta_1 + r_2 T_2 \cos \theta_2 - r_3 T_3 \cos \theta_3 \quad (4.2.36)$$

$$T = T_1 + T_2 + T_3 \quad (4.2.37)$$

Using these three equations and the geometry of Figure 4.2.25 to relate the θ's to α, the ratios T_1/T, T_2/T, and T_3/T were plotted as shown in Figure 4.2.26.

The acceleration limiter is designed so that for the worst-case α (approximately 20°) and the largest spacecraft mass, engine number one just reaches 104 pounds.

Using the above consideration, together with limiter tolerance, accelerometer tolerance, and acceleration loop steady-state error, the following values are obtained.

$$\hat{a}_{max} = 12.58 \text{ ft/sec}^2 \quad (4.2.38)$$

$$\hat{a}_{min} = 4.79 \text{ ft/sec}^2 \quad (4.2.39)$$

A detailed account of these computations is given in References 6 and 7.

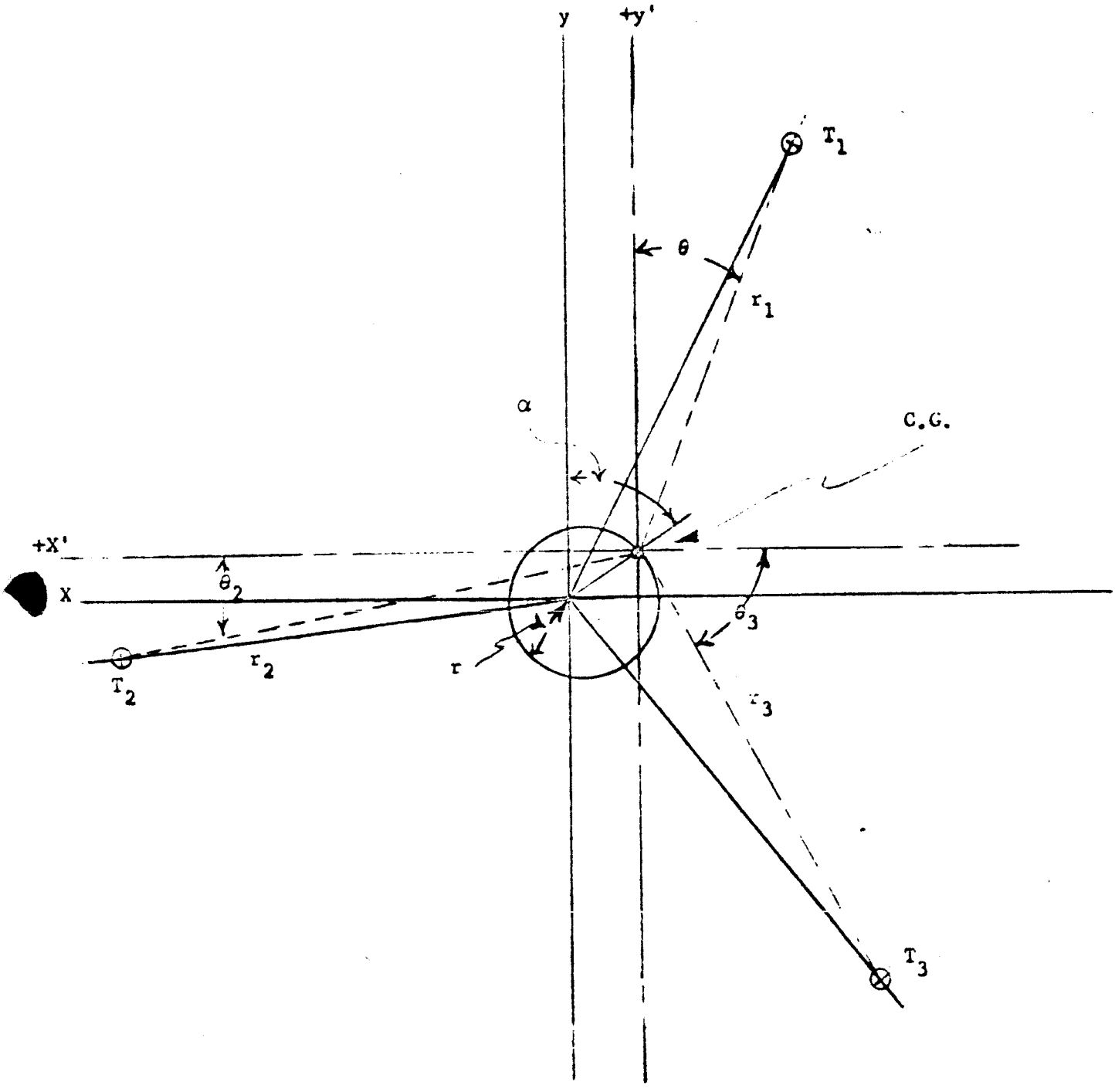

FIGURE 4.2.25

Figure 4.2.26

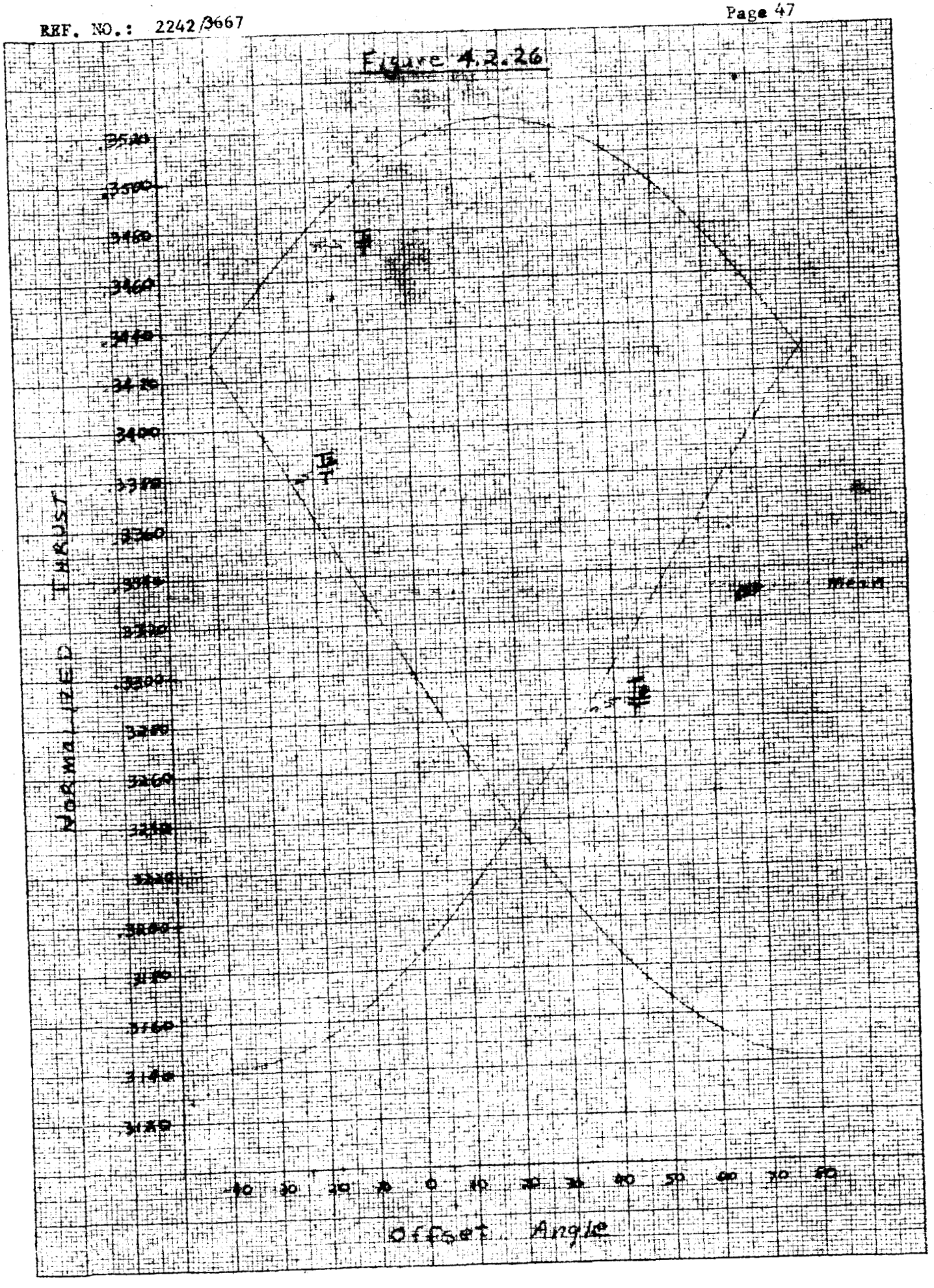

REFERENCES

1. HAC IDC 2242/2780, "Surveyor Coast Phase Attitude Control System", by E. I. Axelband, dated 1 November 1963

2. HAC Specification No. 224836, "Surveyor Angular Alignment Specification", by D. Plummer

3. HAC Specification No. 224510B, "Surveyor Spacecraft System - Functional Requirements", dated February 1962

4. HAC IDC 2242/2232, "Surveyor Flight Control System Reselection of Parameters for Terminal Descent due to Vernier Engine Valve Hysteresis", by S. M. Levy, dated 28 May 1963

5. HAC IDC 2242/79, "Surveyor Midcourse Velocity Control", by E. I. Axelband, dated 20 June 1961

6. HAC IDC 2242/3088, "Surveyor Terminal Descent Command Trajectory Design", by R. N. Crane and G. E. O'Connor, dated 12 November 1963

7. HAC IDC 2242/3206, "Surveyor Attitude and Velocity Control System Parameters for Terminal Descent", by H. D. Marbach, dated 6 January 1964.